

# Advances on Transition Metal Oxides Catalysts for Formaldehyde Oxidation: A

## Review

Abubakar Yusuf <sup>a, b</sup>, Colin Snape <sup>c</sup>, Jun He <sup>a, b \*</sup>, Honghui Xu <sup>d</sup>, Chaojie Liu <sup>a, e</sup>, Ming Zhao <sup>f \*</sup>, George Zheng Chen <sup>a, c, e</sup>, Bencan Tang <sup>a</sup>, Chengjun Wang <sup>g</sup>, Jiawei Wang <sup>h</sup>, Sailesh N. Behera <sup>i</sup>

<sup>a</sup> *Research Group of Natural Resources and Environment, Department of Chemical and Environmental Engineering, The University of Nottingham Ningbo China, Ningbo, PR China*

<sup>b</sup> *International Doctoral Innovation Centre, The University of Nottingham Ningbo China, Ningbo, PR China*

<sup>c</sup> *Faculty of Engineering, University of Nottingham, University Park, Nottingham, NG7 2RD, UK*

<sup>d</sup> *Zhejiang Meteorological Science Institute, Hangzhou, PR China*

<sup>e</sup> *Centre for Sustainable Energy Technologies, Faculty of Science and Engineering, The University of Nottingham Ningbo China*

<sup>f</sup> *School of Environment, Tsinghua University, Beijing 100084, China*

<sup>g</sup> *College of Chemistry and Materials Engineering, Wenzhou University, Wenzhou, PR China*

<sup>h</sup> *Aston Institute of Materials Research, Aston University, Birmingham, B4 7ET, UK*

<sup>i</sup> *Department of Civil Engineering, Shiv Nadar University, Greater Noida, U.P., India*

Correspondence:

Dr Jun He, email: [jun.he@nottingham.edu.cn](mailto:jun.he@nottingham.edu.cn);

Dr Ming Zhao, email: [ming.zhao@tsinghua.edu.cn](mailto:ming.zhao@tsinghua.edu.cn)

1   **Abstract**

2   This review highlights recent advances in the development of transition metal based catalysts for  
3   formaldehyde oxidation, particularly the enhancement of their catalytic activity for low  
4   temperature oxidation. Various factors that enhance low temperature activity are reviewed, such  
5   as morphology and tunnel structures, synthesis methods, specific surface area, amount and type of  
6   active surface oxygen species, oxidation state and density of active sites are discussed. In addition,  
7   catalyst immobilization for practical air purification, reaction mechanism of formaldehyde  
8   oxidation and the reaction parameters affecting the overall efficiency of the reaction are also  
9   reviewed.

10   Keywords:   formaldehyde, transition metal oxides, catalysts, oxidation

## 1. Introduction

Formaldehyde (HCHO) is one of the main sources of hazardous indoor air pollution. Furniture and building materials such as composite wood, particle board, vinyl coverings and adhesives are some of the major indoor sources of HCHO emissions (1,2). A comprehensive review of both the indoor and outdoor sources of HCHO and its concentrations in various indoor environments can be found in the work of Salthammer et al. (3). Exposure to HCHO may cause adverse health effects on humans such as irritation to eyes, nose and throat, headache, fatigue, edema, severe allergic reaction and dermatitis (4,5). In 2006, the International Agency for Research on Cancer (IARC) under the World Health Organization (WHO) classified HCHO as a carcinogen to humans. There are sufficient evidences to ascertain that it causes nasopharyngeal cancer and there are also strong indications that it may also cause sinonasal cancer and leukemia over long term exposure (6). As such there are various international guidelines and recommended thresholds for indoor air HCHO concentrations, a summary of which can be found in the review of Salthammer et al. (3). The WHO proposes a short term HCHO exposure limit (30 minutes) of  $0.1 \text{ mg/m}^3$  for the avoidance of sensory irritation and a long term exposure limit of  $0.2 \text{ mg/m}^3$  for protection against long term health effects (7). Thus, the effective removal of HCHO from indoor air is imperative to improving indoor air quality and safeguarding human health.

Various techniques for HCHO removal have been investigated and reported in the literature, including adsorption (8-12), photo-catalytic oxidation (13-17) and catalytic oxidation (thermal and non-thermal). The effectiveness of physical adsorption of HCHO on adsorbents such as activated carbon (AC) is constrained by the material's maximum adsorption capacity, relative humidity (RH) or moisture deactivation and also by the environmental risk when desorption occurs during regeneration (18,19). Photo-catalytic oxidation using ultraviolet light on the other hand may lead

to the generation of toxic by-products (20). Catalytic oxidation is able to achieve complete conversion of HCHO to H<sub>2</sub>O and CO<sub>2</sub> without the formation of harmful by-products or secondary pollutants (21). This could even be achieved at room temperature especially with noble metal catalysts (22-26), thus making it the most promising HCHO removal technique (18).

Noble metal-based catalysts: Pt, Au, Pd, Rh, Ru and Ag supported on conventional materials such as TiO<sub>2</sub>, SiO<sub>2</sub>, Al<sub>2</sub>O<sub>3</sub> and zeolites (27-35); single transition metals (36-47) and transition metal-based composites (48-51) exhibit excellent HCHO oxidation activities at temperatures lower than 100°C and even at room temperature. Comprehensive reviews on noble metal catalysts for HCHO oxidation have been conducted (4, 25), whilst here a summary of some of the noble metal catalysts and their reaction conditions are presented in Table 1. However, the industrial applications of noble metal catalysts are restricted by their high costs, limited resources and poor thermal stabilities (53). Hence recent research efforts have been focused on the development of relatively cheap materials for low temperature HCHO catalytic oxidation (54-56). More abundant and cost effective metal oxides especially those of the transition metals, including single transition metals and transition metal based composites are shown to be active for HCHO oxidation. However their relatively low activity compared to noble metals catalysts has motivated effort for further improvement. Therefore, the development of highly active and cost effective catalysts for HCHO oxidation is still a major challenge for practical application.

A number of review papers have been published on HCHO removal. Pei and Zhang (52) reviewed chemisorption method and catalytic oxidation of HCHO majorly on noble metal catalysts. The photo-catalytic oxidation of HCHO using TiO<sub>2</sub> as a photo-catalyst both in aqueous and gaseous mediums and the effects of different light sources and photoreactors have also been reviewed in a short article (57). More recently, Bai et al. (4) reviewed the catalysts for HCHO oxidation with a

major focus on the factors affecting the activity of noble metal catalysts. From the literature review, it can be seen that significant progress has been made on improving the activity of transition metal based catalysts and their immobilization for practical application since 2000. However, to the best of our knowledge, the development of transition metal based catalysts for HCHO degradation has not been reviewed in any detail so far. Therefore, we consider this review fills a key gap for this active area of heterogeneous catalysis.

This review focuses exclusively and extensively on recent developments over the past one and half decade towards enhancing the activity of transition metal catalysts for low temperature HCHO oxidation, considering their cost reduction potential, activity and stability. Various factors that enhance their catalytic activities are discussed, including preparation methods, morphology and structure, specific surface area, concentration of surface active oxygen species, oxygen mobility and metal active sites. The influence of reaction parameters such as relative humidity, HCHO concentration and space velocity are also reviewed. The reaction mechanisms of HCHO oxidation on transition metal oxides and their immobilization on suitable substrate materials for application in air purification are also elaborated and finally areas for further investigations to achieve higher activities at low temperatures are proposed.

## **2. Transition metal based catalysts and their performances**

As mentioned earlier, recent research efforts have been focused on the utilization and efficiency improvement of transition metal based catalysts for low temperature oxidation of HCHO. Transition metal oxides are relatively cheap, abundant and have also been presented to be active for HCHO oxidation at low temperatures (21,67,68). Different terminologies such as HCHO removal, conversion, degradation and elimination are used in the literature to refer to the efficiency of HCHO oxidation. Hereinafter, efficiency of HCHO oxidation is referred to as conversion where

oxidation efficiency was reported as a function of CO<sub>2</sub> generation/concentration in the effluent stream and as removal where efficiency was reported based on residual HCHO concentration in the effluent gas stream (see footnotes of Table 1&2).

Some conventional transition metal-based catalysts have been reported to show good catalytic activities for HCHO oxidation. Sekine (2) first demonstrated the catalytic oxidation of HCHO over metal oxide catalysts. Of the investigated catalysts: CoO, MnO<sub>2</sub>, TiO<sub>2</sub>, CeO<sub>2</sub> and Mn<sub>3</sub>O<sub>4</sub>, MnO<sub>2</sub> was described to exhibit the highest catalytic activity. Metal oxides in the conventional bulk form possess low catalytic activity for HCHO oxidation owing to inferior surface properties (69). On the contrary, specially synthesized nanostructured transition metal catalysts of similar compositions to their bulk counterparts exhibit improved morphologies and surface properties and hence higher activities for HCHO oxidation (21,70). As such, current investigations on transition metal-based catalysts are focused on improving and developing materials with enhanced morphologies and structures. The structure of these catalysts and their morphologies improve their activity through the improvement of parameters (discussed in Section 4) such as specific surface area, high surface reducibility, porosity, active surface species, active lattice and surface adsorbed oxygen species and tunnel size and structure (54,55). Transition metal-based catalysts for HCHO oxidation found in the literature could basically be classified as single/mono-metal and composite metal oxides. A summary of both group of catalysts and their activities and conditions of reaction are respectively presented in Table 2 and 3.

## 2.1 Single transition metal based catalysts

### 2.1.1 Manganese oxide based catalysts

Manganese oxide is the most widely explored transition metal catalyst for HCHO oxidation owing to its high catalytic activity, thermal stability, existence in various crystal morphologies such as  $\alpha$ -

,  $\beta$ -,  $\gamma$ - and  $\delta$ - $\text{MnO}_x$  (71) and several tunnel assemblies (1D tunnels, layered structures such as birnessite and buserite and 3D spinel tunnel structures) (72). Chen et al. (55) studied the influence of tunnel structures of various manganese oxide catalysts (pyrolusite, cryptomelane and todorokite) on HCHO oxidation. Cryptomelane displayed the highest activity with 100% HCHO conversion at 140°C, 400 ppm HCHO concentration, and a space velocity of 18,000 mL/g·h, while 20 and 40% conversions were attained by pyrolusite and todorokite, respectively, under similar reaction conditions. Tunnel size and structure were shown to be the determinant factors affecting activity other than factors such as specific surface area, degree of crystallinity, surface reducibility and average oxidation states of the catalysts. Similarly, Zhang et al. (19) attributed the high HCHO catalytic activity of  $\delta$ - $\text{MnO}_2$  to its interlayer and tunnel structures which help in expediting adsorption and diffusion to and from the catalyst's active sites. These results indicate that activity is closely related to morphological and structural properties of the catalyst.

Tian et al. (54) investigated the impact of synthesis temperature on birnessite type manganese oxide catalysts. A general trend of catalytic activity rise was observed with increasing synthesis temperature from 80 to 120°C. The catalyst synthesized at 120°C exhibited the highest activity with a HCHO conversion of 100% at 100°C. This observed high activity was attributed to higher surface reducibility, specific surface area, crystallinity and porosity compared to other catalysts synthesized at different temperatures. Wang et al. (73) studied the effect of  $\text{H}_2\text{O}$  molecules on the activity of birnessite manganese for HCHO oxidation at room temperature and indicated that activity depends on the amount of both adsorbed  $\text{H}_2\text{O}$  molecules and interlayer hydroxyl and  $\text{H}_2\text{O}$  molecules present in the catalyst. Interestingly, as the drying temperature increases from 30 to 500°C, so does the specific surface area, but activity dramatically decrease as displayed in Figure 1(a) due to the reduction in water content. This result indicates that the activity of birnessite is

more a function of the interlayer H<sub>2</sub>O molecule content than specific surface area. The presence of H<sub>2</sub>O molecules enhances adsorption of HCHO molecules on the surface, conversion and desorption of intermediates from the catalyst's surface.

Furthermore, the effect of manganese vacancy ( $V_{Mn}$ ) on the activity of birnessite-type MnO<sub>2</sub> was studied (74). Their results indicate that the presence of  $V_{Mn}$  improves the content of the surface adsorbed oxygen containing species facilitated by the presence of interlayer K<sup>+</sup>, which helps in charge imbalance compensation caused by the created vacancy. The effect of surface pores created by the modification of birnessite-MnO<sub>2</sub> with nitric acid and tetra-ammonium hydroxide on HCHO oxidation was also investigated (75). The created defects as proposed by the authors served as sites for activation of molecular oxygen and H<sub>2</sub>O, hence resulting in the increased density of active surface oxygen species and activity of the modified catalyst.

Tian et al. (56) also examined the effect of synthesis reaction temperature on the catalytic activities of various cryptomelane manganese octahedral molecular sieve K-OMS-2 catalysts. The K-OMS-2 nanoparticle catalyst prepared at room temperature exhibited a higher catalytic activity compared to K-OMS-2 nanorod structured catalyst prepared at 100°C. The former attained 64% HCHO conversion at the reaction temperature of 100°C was due to the existence of a higher proportion of pore channels compared to the 10% accomplished by the latter under the same reaction conditions. Tian et al. (36) studied the relationship between textural properties and catalytic activity of the cryptomelane manganese oxide catalyst, and showed that a resultant increase in textural properties (specific surface area and pore volume) as a result of synthesis temperature increment from 15 to 70°C led to a dramatic improvement in catalytic activity.



Three dimensional mesoporous  $\text{MnO}_2$  (3D  $\text{MnO}_2$ ) catalysts prepared via nanocasting route using KIT-6 hard template, which retain the mesoporous properties of the template were shown to be promising for HCHO oxidation (76). The mesoporous structure, high specific surface area and large number of surface active  $\text{Mn}^{4+}$  ions enhanced its high activity compared to the corresponding  $\alpha$ - $\text{MnO}_2$  and  $\beta$ - $\text{MnO}_2$  nanorod catalysts. Complete HCHO oxidation to  $\text{H}_2\text{O}$  and  $\text{CO}_2$  was accomplished at  $130^\circ\text{C}$  with 3D  $\text{MnO}_2$  while same conversion was achieved at  $140^\circ\text{C}$  and  $180^\circ\text{C}$  respectively with  $\alpha$ - $\text{MnO}_2$  and  $\beta$ - $\text{MnO}_2$  under similar reaction conditions. This indicates that activity is closely related to morphological structures of the catalyst. The catalytic activities of  $\alpha$ ,  $\beta$ ,  $\gamma$  and  $\delta$  phase structures of  $\text{MnO}_2$  were also investigated (19). The following order of activity for complete HCHO oxidation was established:  $\delta > \alpha > \gamma > \beta$ -  $\text{MnO}_2$ . Complete HCHO oxidation was attained at  $80^\circ\text{C}$  on  $\delta$ - $\text{MnO}_2$ . Its high activity was suggested to be a function of its abundant concentration of lattice oxygen species (see section 4.3 for further discussion on the roles active surface oxygen species) and 2D layered structure, the latter of which enables easy adsorption and diffusion of HCHO.

Chen et al. (21) prepared mesoporous hollow and honeycomb structured  $\text{K}_x\text{MnO}_2$  nanospheres. The former displayed higher activity of up to 100% HCHO removal at  $80^\circ\text{C}$ , while the latter attained similar removal efficiency at  $100^\circ\text{C}$  under similar reaction conditions. Catalytic activity of hollow structured  $\text{K}_x\text{MnO}_2$  nanospheres was attributed to its porosity and the ability to retain HCHO in its pores for a longer period compared to honeycomb structured catalyst. Zhou et al. (77) examined the catalytic activity of various structures of Mn and the following order of decreasing activity was established at reaction temperature below  $120^\circ\text{C}$ : cryptomelane  $\text{Mn}_2\text{O} >$  birnessite  $\text{Mn}_2\text{O} >$  ramsdellite  $\text{Mn}_2\text{O} >$  monoclinic  $\text{MnOOH}$ . However, birnessite turns out to exhibit better activity for complete HCHO oxidation at higher temperature, achieving 100% removal at  $140^\circ\text{C}$

while cryptomelane at 160°C under similar conditions. This was possibly a result of weakened HCHO adsorption on cryptomelane at lower temperature as suggested by the authors.

### *2.1.2 Cobalt oxide based catalysts*

Cobalt oxide is another important transition metal-based oxide that has recently been attracting attention for low temperature VOC catalytic applications. Similar to  $\text{MnO}_x$ ,  $\text{Co}_3\text{O}_4$  also exhibit various morphologies which include nano-fibers (78), nano-sheets, nano-cubes, nano-rods (79) and the morphologies influence its catalytic activity through the exposure of catalytically active surface sites (70). The activity of Nano-, 2D- and 3D- $\text{Co}_3\text{O}_4$  structures for complete HCHO oxidation was compared and the following order of reactivity was established: 3D- $\text{Co}_3\text{O}_4$  > 2D- $\text{Co}_3\text{O}_4$  > nano- $\text{Co}_3\text{O}_4$  (70). The superior activities of 3D and 2D- $\text{Co}_3\text{O}_4$  was ascribed to their mesoporous channel structure which enables easy diffusion of reactants to undergo reaction on the active surface compared to the non-porous nano- $\text{Co}_3\text{O}_4$ ; in addition, the best performance of 3D- $\text{Co}_3\text{O}_4$  was closely related to its abundant surface adsorbed oxygen species, large specific surface area and exposed active  $\text{Co}^{3+}$  species on the (2 2 0) crystal face. Similarly, Ma et al. (51) indicated that 2D- $\text{Co}_3\text{O}_4$  composed mainly of active  $\text{Co}^{3+}$  species on the (1 1 0) facet was able to achieve 20.3% HCHO oxidation at room temperature.

Fan et al. (67) investigated the effect of precipitants on the activity of  $\text{Co}_3\text{O}_4$  catalysts. The catalysts synthesized using carbonates and bicarbonates displayed better textural properties and superior catalytic activities. The catalyst produced from  $\text{KHCO}_3$  reached 100% HCHO conversion at 90°C, compared to 120°C and 130°C for those prepared from KOH and  $\text{NH}_3\cdot\text{H}_2\text{O}$ , respectively. Recently, Wu et al. (78) described the utilization of porous  $\text{Co}_3\text{O}_4$  nanofibers prepared by spiral electrospinning and controlled calcination (500°C) as highly active catalysts for HCHO oxidation. Complete oxidation was accomplished at 98°C under a space velocity of 30,000 mL/g·h and it was

shown to be highly stable for up to 160 hrs. Its activity was attributed to its high specific surface area and large pore volume which provided more active sites for the reaction.

Despite the reported influence of morphological structure on the activity of  $\text{Co}_3\text{O}_4$  based catalysts, very few structures have been exploited for HCHO oxidation. There is therefore the need for further work to investigate other structures such as nano-sheets, nano-cubes, nano-rods and the extent to which they can influence other properties such as specific surface area, porosity and exposure of active metal sites and active oxygen species for improved low temperature HCHO oxidation.

### *2.1.3 Other metal oxides*

Beside manganese and cobalt based catalysts, other metal oxides have been investigated in the literature. Xia et al. (69) synthesized 3D ordered rhombohedra  $\text{Cr}_2\text{O}_3$  using assisted ultrasound nanocasting in the presence of 3D mesoporous silica (KIT-6) as template. The catalyst attained up to 90% HCHO conversion at  $117^\circ\text{C}$ . The ultrasound assisted synthesis played a major role in improving the characteristics and activity of the catalyst compared to similar catalysts synthesized in the absence of ultrasound. Huang et al. (80) first recounted the use of bifunctional Eu-doped  $\text{CeO}_2$  with both thermal- and photo-catalytic oxidation capabilities for HCHO oxidation. Doping Eu onto  $\text{CeO}_2$  dramatically enhanced its HCHO oxidation activity and complete oxidation temperature was reduced from  $310^\circ\text{C}$  on pure  $\text{CeO}_2$  to  $120^\circ\text{C}$  on 4% Eu doped  $\text{CeO}_2$ . Catalytic activity was promoted through oxygen vacancy creation on the surface of  $\text{CeO}_2$ , greater redox ability, more abundant surface active  $\text{Ce}^{3+}$  and enhanced surface reaction. The created defects provide more sites for oxygen activation hence providing more active surface oxygen species for reaction. In addition, the catalysts exhibited an outstanding stability of up to 100 hrs on stream without any sign of deactivation. Similarly, Zeng et al. (81) demonstrated that hydrogenation

treatment of  $\text{TiO}_2$  and C- $\text{TiO}_2$  improved their activity through the creation of more surface oxygen vacancy and surface hydroxyl groups. The untreated catalysts virtually displayed no activity for HCHO oxidation in a static chamber reaction after 4 hrs at room temperature in the absence of light illumination, while the treated catalysts including H- $\text{TiO}_2$  and H-C- $\text{TiO}_2$  were able to respectively attain 53% and 57% removal under similar reaction conditions.

In general, manganese and cobalt based catalysts were demonstrated to be active compared to other transition metals catalysts for HCHO oxidation. However, not much work has been done on other transition metals. In order to explore their full potentiality as viable catalysts, further work is needed to explore their utilization for low temperature HCHO oxidation. In addition, more work is required to explore surface oxygen vacancy or defects creation using various dopants to improve oxygen activation ability of metal oxide catalysts, to enrich active surface oxygen concentration for enhanced low temperature reaction.

## 2.2 Transition metal-based composites/mixed oxides

Transition metal-based composites have been widely applied in the control of pollutants such as CO (83,84) and ammonia (85). Composite catalysts for HCHO oxidation have also been investigated and reported in the literature. These catalysts are generated by co-synthesis of two transition metals oxides or the addition of other metal oxides either by co-precipitation (48,86) or by other synthesis methods such as nanocasting (51). Composite catalysts were shown to exhibit superior catalytic activities compared to the corresponding single materials synthesized using similar procedure. This is due to synergistic or promotional influence of improved oxidation capabilities either through higher surface oxygen mobility, creation of more oxygen vacancies (48,86) or enhancing charge transport during redox cycles (87). To improve oxygen vacancy formation in a composite catalysts and reduce the energy requirement for such, it was suggested

that the dopant should possess weaker M-O bonds; have larger radius and possess lower electronegativity (88). Various composites such as  $\text{MnO}_x\text{-CeO}_2$  (48,86),  $\text{Co}_3\text{O}_4\text{-CeO}_2$  (51),  $\text{MnO}_2\text{-Fe}_2\text{O}_3$  (89),  $\text{CuO-MnO}_2$  (51,89),  $\text{MnO}_x\text{-SnO}_2$  (90),  $\text{Co}_3\text{O}_4\text{-ZrO}_2$  (91) and Co-Mn oxide (68) have been studied for HCHO oxidation.

### 2.2.1 $\text{MnO}_x\text{-CeO}_2$ composites

The composites of Mn and Ce oxides were shown to be active for HCHO oxidation owing to the synergistic effect of Mn high activity and  $\text{O}_2$  storage capacity of ceria. In addition, the composites aid in attaining higher oxidation states for Mn (83,92) which is vital for HCHO oxidation (87). Formation of solid solution between Mn and Ce is also critical to achieving synergistic influence through  $\text{O}_2$  transfer mechanism (48,86). Solid solution was shown to be attained in the Mn-Ce molar ratio ( $\text{Mn}/(\text{Mn} + \text{Ce})$ ) range of 0.3 to 0.5, with 0.5 molar ratio being the optimum composition (48,86,93) and the solubility limit for the substitution of Ce ions by Mn ions in the composite (53).

Tang et al. (86) indicated that the manifestation of synergy in  $\text{MnO}_x\text{-CeO}_2$  solid solution composite, which enables the composite to attain complete HCHO conversion at lower temperature ( $100^\circ\text{C}$ ) compared to pure  $\text{MnO}_x$  and  $\text{CeO}_2$ . The synergy was attained through a series of redox cycles ( $\text{Mn}^{4+}/\text{Mn}^{3+}$  and  $\text{Ce}^{4+}/\text{Ce}^{3+}$ ) involving the activation of molecular oxygen by Ce and its transfer to Mn. The optimum calcination temperature for solid solution stability was shown to be  $550^\circ\text{C}$ , above which activity decreased owing to phase segregation. In another investigation, Tang et al. (48) further highlighted that above Mn-Ce molar ratio of 0.5,  $\text{MnO}_x$  crystallizes out of the solid solution, with a consequent drastic reduction in catalytic activity, which is in conformity with the findings of Li et al. (93). However, higher total decomposition temperature of  $270^\circ\text{C}$  was reported by Li et al. (93) for  $\text{Mn}_{0.5}\text{Ce}_{0.5}\text{O}_2$ . Nonetheless, the catalysts were able to totally oxidize

HCHO at room temperature in the presence of 506 ppm ozone ( $O_3$ ) in the feed stream. The ozone molecules enhance the reaction by dissociating on the catalyst's surface and providing enough atomic oxygen species to drive the reaction (93).

Quiroz et al. (53) studied the impact of acid treatment over  $MnO_x$ - $CeO_2$  composite for HCHO oxidation. Their results indicated that the treatment had no pronounced effect on the textural and redox properties of the composites within the solubility limit of Mn (Mn molar ratio  $\leq 0.5$ ) in  $CeO_2$ . However, at higher Mn molar ratio (0.7 and 1) when  $MnO_2$  began to crystallize out of the solid solution, significant improvement in catalytic activity was observed owing to the increased specific surface area and higher oxidation state of surface Mn. It is important to mention that while textural properties of the solid solution were not altered by the acid treatment, the oxygen transfer ability of  $CeO_2$  was significantly hampered by the formation of  $Ce(SO_4)_2$  resulting into a drastic reduction in activity. Therefore, acid treatment has positive effects on pure  $MnO_2$  and an inhibitive effect on the synergy of the solid solution composites. The modification of birnessite-structured  $MnO_2$  with ceria for HCHO oxidation was also reported in the literature (94). The incorporation of cerium ions inhibited the growth of  $MnO_2$  crystals leading to particle size reduction and increase in specific surface area, as the amount of doped ceria increases. The doping led to the increase in the amount of oxygen vacancies and the rate of molecular oxygen activation into surface adsorbed oxygen species ( $O_2^-$ ,  $O^-$  or terminal hydroxyl (OH) group (74)). The catalyst with the highest ratio of surface adsorbed oxygen to lattice oxygen exhibited the best catalytic performance. At higher ceria doping ( $Ce$ - $MnO_2$ , molar ratio 5:10), the birnessite structure collapsed leading to decrease in catalytic activity.

Tang et al. (48) further demonstrated that impregnating Pt on  $MnO_x$ - $CeO_2$  composite significantly improved its activity by attaining 100% HCHO conversion at room temperature as shown in Table

1. It is noteworthy to mention that the formed composite (Pt/MnO<sub>x</sub>-CeO<sub>2</sub>) was prone to deactivation with increasing HCHO concentration. Its activity dropped from 100% conversion at 30 ppm to 54% in the presence of 580 ppm HCHO at room temperature as shown in Figure 2. Meanwhile the same authors (86) showed that MnO<sub>x</sub>-CeO<sub>2</sub> composite was stable for complete HCHO oxidation over 48 hrs without any sign of deactivation at similar concentration (580 ppm). It should however be noted that the latter experiment was conducted at 100°C and the high temperature could aid the decomposition of intermediate species while the former was conducted at room temperature. This indicates that Pt might be prone to deactivation by HCHO at higher concentration, which needs to be investigated further.

#### 2.2.2 Co<sub>3</sub>O<sub>4</sub>-CeO<sub>2</sub> composites

Ma et al. (51) investigated the oxidation of HCHO at room temperature on 2D-Co<sub>3</sub>O<sub>4</sub>-CeO<sub>2</sub> composites. They discovered that no synergy or activity improvement was realized by the formed 2D-Co<sub>3</sub>O<sub>4</sub>-CeO<sub>2</sub> composites and that 2D-Co<sub>3</sub>O<sub>4</sub> was more active than the composites with respective HCHO conversions of 13.2% and 20.3% at room temperature. It should however be noted that no solid solution formation was observed in the 2D-Co<sub>3</sub>O<sub>4</sub>-CeO<sub>2</sub> composites, which is a phenomenon reportedly required for achieving synergy through ceria O<sub>2</sub> transfer mechanism (48,86). The incorporation of Au in the composite (2D-Au/Co<sub>3</sub>O<sub>4</sub>-CeO<sub>2</sub>) improved the composite's activity to 50% conversion at room temperature (Table 1) by promoting desorption of surface active oxygen species (51). Liu et al. (50) presented the evidence of solid solution formation in 3D ordered macroporous (3DOM) CeO<sub>2</sub>-Co<sub>3</sub>O<sub>4</sub> catalysts with low loading of Co<sub>3</sub>O<sub>4</sub>. However, the 3D-CeO<sub>2</sub>-Co<sub>3</sub>O<sub>4</sub> catalysts with various Ce-Co molar ratios were shown to possess low catalytic activities. Loading Au particles (3 wt. %) on the composites distinctively improved their catalytic activities, and in fact all the Au supported composites were able to completely convert HCHO into

CO<sub>2</sub> and H<sub>2</sub>O below 65°C. The composites (3D Au/CeO<sub>2</sub>-Co<sub>3</sub>O<sub>4</sub>), with lower Co content in CeO<sub>2</sub>-Co<sub>3</sub>O<sub>4</sub> in the region solid solution, presented better activity in this study. When higher Co molar ratios was employed, segregation between CeO<sub>2</sub> and Co<sub>3</sub>O<sub>4</sub> occurred, which led to weaker interaction and thus reduced the activity of the Au/CeO<sub>2</sub>-Co<sub>3</sub>O<sub>4</sub> catalysts.

### *2.2.3 Co-Mn oxides Composites*

The composites of Co and Mn oxides were also studied and shown to be more active than the individual pure oxides for HCHO complete oxidation (95). Favorable synergy was obtained due to the abundant surface adsorbed oxygen species generated by the oxygen vacancies created in the Co-Mn oxides solid solution. Textural and redox properties were also shown to be affected by the synthesis method employed. Co-precipitation synthesis produced a more active catalyst with higher specific surface area, higher relative content of surface adsorbed oxygen species and surface active manganese (Mn<sup>4+</sup>) that completely oxidized HCHO at 75°C compared to 100°C over that synthesized using sol-gel method.

Wang et al. (68) further studied the efficiency of the cycling “storage-oxidation” process for HCHO oxidation using 3D ordered mesoporous Co-Mn oxides composite (3D-Co-Mn) synthesized using KIT-6 template and that of Co-Mn oxides composite synthesized using co-precipitation. During the storage process, the catalysts were first exposed to a feed stream of O<sub>2</sub> and HCHO; subsequently, the stored HCHO was oxidized in a flow of O<sub>2</sub> at elevated temperature to evaluate its activity. The 3D-Co-Mn oxides composite was shown to have superior storage capacity of up to 0.8 mmol/g-catalyst and HCHO complete oxidation temperature of 70°C, compared to the storage capacity of 0.428 mmol/g-catalyst and HCHO complete oxidation temperature of 75°C respectively achieved by co-precipitated Co-Mn oxides composite. The



excellent activity of 3D-Co-Mn oxides composite was attributed to its larger specific surface area and ordered mesoporous structure. Lu et al. (96) studied HCHO oxidation over  $\text{MnO}_x\text{-Co}_3\text{O}_4\text{-CeO}_2$  composites and found out that the incorporation of  $\text{MnO}_x$  into  $\text{Co}_3\text{O}_4\text{-CeO}_2$  greatly improved its textural properties and the amount of available surface active oxygen species, resulting in an improvement in catalytic activity.

### 2.2.3 Other Composites

Other composites such as  $\text{MnO}_x\text{-SnO}_2$  (90) and zirconia supported cobalt oxide catalysts (91) have been reported in the literature. Wen et al. (90) showed that the redox properties of  $\text{MnO}_x\text{-SnO}_2$ , which were in turn influenced by the preparation method, played a crucial role in determining its activity. Their experimental results highlighted that higher oxidation states of Mn were more active in HCHO oxidation. The dominant oxidation state of Mn in the composite synthesized using redox co-precipitation was  $\text{Mn}^{4+}$  while  $\text{Mn}^{3+}$  was the main state in the co-precipitated composite, which accounted for the difference in their activities as shown in Table 3. This is in agreement with other reported literatures for the active state of Mn for HCHO oxidation (76,86). Lu et al. (87) investigated the catalytic performance of graphene- $\text{MnO}_2$  (G-Mn) hybrid for complete oxidation of HCHO. The G-Mn hybrid catalyst achieved complete HCHO conversion at  $65^\circ\text{C}$ , compared to  $140^\circ\text{C}$  for pure  $\text{MnO}_2$  and the completely inactive graphene (G) nanosheets. The hybrid system exposed more  $\text{Mn}^{4+}$  active sites, enhanced charge transport during Mn redox cycle and offered a larger amount of surface HYDROXYL species which eased HCHO oxidation and improved activity.

## 3. Catalyst immobilization on porous materials for practical HCHO oxidation

For practical applications, deployment of powdered form materials especially nanosized, gives rise to engineering challenges such as dust contamination and nanoparticle leaching in flue gas streams

(82). Therefore, catalysts immobilization on porous materials with low air pressure drop is considered viable for air purification processes. A variety of porous materials with low air resistance including polyethylene terephthalate (PET) (18), polyester particulate filter (97) and porous cellulose fiber (82) have been used as supporting materials for immobilizing nanoparticle catalysts for HCHO oxidation. A summary of the activity of these immobilized catalysts is presented in Table 4. Wang et al. (18) reported the in-situ coating of  $\delta$ -MnOx nanosheet on the surface of PET first through surface reaction followed by in-situ deposition. The formed composite which is light with low air resistance and high specific surface area, proved highly active and stable for low concentration HCHO ( $0.6 \text{ mg/m}^3$ ) oxidation at room temperature for 10 hrs. Sidheswaran et al. (97) supported Mn based catalyst with 84% nsutite, 2% cryptomelane and 13% manjiroite composition on the surface of a thin polyester particulate filter for heating ventilation and air conditioning (HVAC) and evaluated its performance for HCHO oxidation. Experimental results indicated that stable single pass HCHO oxidation with over 80% removal efficiency at room temperature was achieved continuously for 35 days for both high and low face velocities close to typical building air ventilation systems.

Zhou et al. (82) likewise demonstrated an in situ deposition of MnO<sub>2</sub> nanosheets on cellulose fiber composite (8.86 wt.% MnO<sub>2</sub>/cellulose fiber) and showed that even though birnessite powder is slightly more active than the composite (100% and 99.1% at 140°C, respectively), the composite is about 19 times more active in terms of HCHO removal per mg of MnO<sub>2</sub>. However, the observed difference could supposedly be attributed to the removal/adsorption capacity of cellulose fiber and not necessarily HCHO conversion as CO<sub>2</sub> generation and catalytic activity of the cellulose fiber were not monitored in the experiment. Li et al. (98) and Dai et al. (71) respectively utilized AC for immobilizing birnessite-MnO<sub>2</sub>. In both cases, HCHO was completely converted into CO<sub>2</sub> in a

static reaction chamber. However, the conversion patterns in the individual experiments were such that the concentration of HCHO sharply dropped in the first 60 mins with little corresponding CO<sub>2</sub> generation, possibly indicating that the molecules were actually adsorbed onto the surface of AC. The adsorbed molecules were consequently and slowly converted into CO<sub>2</sub> over 6 hrs (98) and 9 hrs on birnessite-MnO<sub>2</sub>/AC (71) respectively as shown in Figure 3(a&b). Similar patterns were observed over unsupported birnessite as shown in Figure 1(b) (73). In contrast, simultaneous HCHO conversion and CO<sub>2</sub> generation were observed over modified birnessite with manganese vacancies and up to 81.7% conversion was attained in the first one hour of the static experiment (74). This indicates that the HCHO is instantaneously converted into CO<sub>2</sub>, as opposed to the AC supported birnessite (71,98) in which the HCHO is adsorbed onto the AC and subsequently converted over time. Few immobilized transition metal-based catalysts for HCHO oxidation have been reported as presented in Table 4; therefore, further investigations are required to evaluate more effective substrate materials for immobilization and to understand their interactions with the catalysts and effectiveness for practical application in air purification process. In addition, these materials need to be tested under indoor conditions in air purifiers or HVAC systems and evaluate the effect of conditions such as particle leaching, dust contamination, relative humidity and temperature variation, on the effectiveness and stability of these materials.

#### **4. Influence of catalyst based factors on HCHO oxidation efficiency**

The effectiveness of HCHO oxidation process is majorly related to the activity/reactivity of the catalyst deployed and other reaction parameters such as temperature, concentration, space velocity, catalyst mass and relative humidity. Catalytic activity is in turn influenced by a number of physicochemical properties which include structure and morphology, preparation or synthesis method, degree of crystallinity, surface reducibility, specific surface area, amount of active oxygen

species and active metal sites (54). A combination of these properties is decisive for high catalytic activity and for an effective HCHO oxidation at low reaction temperature.

#### 4.1 Influence of synthesis methods and conditions on textural properties, morphology and activity

Several conventional preparation methods can be used to synthesize catalysts for HCHO oxidation including sol-gel method (56), precipitation and co-precipitation (86,97). Recent researches have mainly focused on improving and modifying catalysts preparation methods to enhance their performance and catalytic activities through the utilization of synthesis techniques such as hydrothermal synthesis (77), electrospinning (78), electrodeposition (80) and hard template nanocasting (70,76). Synthesis methods and reaction conditions are able to tailor catalysts' textural and surface properties, structures and morphologies (as shown in Figure 4 (77)) and hence influence their catalytic activity (36,54) as shown in. For instance, the utilization of ultrasound assisted nanocasting of 3D-Cr<sub>2</sub>O<sub>3</sub> using KIT-6 as template helps in enhancing the penetration of precursor materials into the mesoporous structure of KIT-6, which proved efficient in improving its specific surface area, pore volume and mesoporosity compared to 3D-Cr<sub>2</sub>O<sub>3</sub> synthesized without the aid of ultrasound (69). Zhang et al. (19) highlighted that by varying reaction conditions in a hydrothermal synthesis, various crystal structures of MnO<sub>2</sub> including:  $\alpha$ - and  $\delta$ -MnO<sub>2</sub>;  $\beta$ - and  $\gamma$ -MnO<sub>2</sub>, with entirely different properties can respectively be produced from the same starting materials.

Reaction temperatures in hydrothermal synthesis have tremendous effects on morphology and structural evolution of structured manganese catalysts. Tian et al. (54) highlighted that the reaction temperature greatly affects the crystallinity, surface reducibility, specific surface area and activity of birnessite structured manganese oxide catalysts. At low synthesis temperature of 80°C, poorly

crystalline birnessites were produced, whilst the birnessites were transformed into well-crystalline structures when reaction temperature was increased to 100°C, thereby increasing its activity. However, higher temperature (140°C) led to decomposition of the birnessite structure as a result of excessive reduction of  $\text{Mn}^{7+}$  by benzyl alcohol during the synthesis. Zhou et al. (77) also observed that birnessites structure obtained at 120°C synthesis temperature transformed into monoclinic  $\text{MnOOH}$  at 150°C and eventually collapsed into 1D  $\text{MnOOH}$  nanorods at 180°C as shown in Figure 4. Similarly, a correlation between synthesis temperature and catalyst's morphology for cryptomelane-type manganese octahedral molecular sieve (K-OMS-2) was reported by Tian et al. (56). The morphologies of the K-OMS-2 catalysts changed from nanoparticles at room temperature to nanorods at reaction temperatures of 80-100°C and to nanowires at 120°C.

Tian et al. (36) reported that essential properties of cyptomelane catalyst such as morphology, crystallinity, specific surface area and pore structure could be tailored by manipulating the hydrothermal synthesis temperature. Increasing synthesis temperature distinctively raised the crystallinity and textural properties of the catalyst. However, too high temperatures diminished crystallinity and this is in agreement with the findings of Tian et al. (54) for birnessite manganese catalysts. Textural properties such as specific surface area and pore volume were also shown to vary with the synthesis temperature. An increase in the synthesis temperature led to a dramatic improvement in textural properties: specific surface area and pore volume increased from 68  $\text{m}^2/\text{g}$  and 0.2  $\text{cm}^3/\text{g}$  at synthesis temperature of 15°C, to 206  $\text{m}^2/\text{g}$  and 0.3  $\text{cm}^3/\text{g}$  at 70°C, respectively. Such an improvement in textural properties in turn led to enhancement in catalytic activity.

Calcination temperature was also demonstrated to be very critical for catalysts structural stability and activity. Wang et al. (73) indicated that between 30 and 300°C only a little change was

observed in the sizes of birnessite nanospheres and that the structure was prevented from collapsing by interlayer  $K^+$  and  $H_2O$  molecules present. However, when the calcination temperature reached up to  $500^\circ\text{C}$ , the layered structure of birnessite completely collapsed and transformed into cryptomelane with a  $2 \times 2$  tunnel structure due to the loss of interlayer  $H_2O$  molecules. The calcination temperature of composite  $MnO_x\text{-CeO}_2$  prepared using modified co-precipitation was shown to greatly influence its catalytic activity for HCHO oxidation (86). As the temperature rises from  $300\text{-}500^\circ\text{C}$ , the relative amount of surface active  $Mn^{4+}$  and lattice oxygen also rises, however at higher temperature ( $700^\circ\text{C}$ ) both the activity and the relative amount of lattice oxygen dramatically decreased due to phase segregation evident by the appearance of  $MnO_2$  crystals in the otherwise solid solution composite. Likewise, Wu et al. (78) indicated that high calcination temperatures ( $600\text{-}800^\circ\text{C}$ ) led to the decrease in the activity of  $Co_3O_4$  nanofibers as a result of aggregation growth and collapse of the catalyst's mesoporous structure.

The utilization of templates and surfactants in catalysts synthesis for HCHO oxidation is also attracting attention. When templates are deployed in catalyst preparation, the catalyst's structures and morphology could easily be manipulated to enhance their catalytic activities (56,76) and replicate the characteristics of the template materials used. While Shi et al. (95) demonstrated that Co-Mn oxides composites prepared using co-precipitation method were far more active than those prepared using sol-gel method, the same group (68) further disclosed that 3D mesoporous Co-Mn oxides synthesized using KIT-6 hard template possessed superior activity owing to their better textural properties. Similarly, the synthesis of 3D- $Cr_2O_3$  (69), 3D- $Co_3O_4$  (70) and 3D- $MnO_2$  (76) have been demonstrated using KIT-6 molecular sieve hard template for HCHO oxidation. The presence of the template improved the mesoporous structure and specific surface area and exposes more active sites thereby enhancing catalytic activity. Other mesoporous structures including 2D-

MnO<sub>2</sub> (99) and 2D-Co<sub>3</sub>O<sub>4</sub> (51,70) have been prepared using SBA-15 hard templates, which turned out to be more active than the corresponding non-porous materials but less active than their 3D-counterparts. Furthermore, Tian et al. (56) highlighted that highly active nanoparticle cryptomelane (K-OMS-2) catalyst could be synthesized at room temperature with the aid of cetyltrimethylammonium bromide (CTAB) surfactants without necessarily the use of high reaction temperature as earlier reported (36).

Acidity of the reaction medium and the type of acid deployed in controlling the pH have significant effects on the morphology of manganese based catalysts. Chen et al. (21) showed that mesoporous hollow and honeycomb K<sub>x</sub>MnO<sub>2</sub> nanospheres with varying properties and activities could be produced by varying the ratio of KMnO<sub>4</sub> and oleic acid during the synthesis process. Zhou et al. (77) revealed that introducing H<sub>2</sub>SO<sub>4</sub> (decreasing the pH) into a reaction medium that would otherwise produce birnessite structured manganese led to the production of cryptomelane structured manganese. However, the type of anions present in the acid is also critical in determining the resultant morphology under similar conditions. While the addition of H<sub>2</sub>SO<sub>4</sub> led to cryptomelane structure, addition of H<sub>3</sub>PO<sub>4</sub> and HNO<sub>3</sub> produced birnessite and ramsdellite structured manganese, respectively as shown in Figure 4. This shows that different anions play dissimilar roles in channeling the mechanism of crystal formation towards a particular morphology.

#### 4.2 Influence of catalyst's morphology on activity

Catalysts' morphology and structure play an important role in promoting catalytic activities. Control over the morphological structure of catalysts is able to influence other properties such as pore size, specific surface area and the exposure of available surface active sites. The activity of manganese oxide catalysts with square tunnel structures (pyrolusite, cryptomelane and todorokite)

is majorly affected by their tunnel sizes (55). Similarly the available surface active sites depend on the nature of the catalysts. 3D-  $\text{MnO}_2$  catalyst have more exposed  $\text{Mn}^{4+}$  on its crystal lattice plane thereby improving its activity compared to the one-dimensional  $\alpha\text{-MnO}_2$  and  $\beta\text{-MnO}_2$  nanorod materials (76).

Chen et al. (55) investigated the effect of  $\text{MnO}_x$  tunnel structure on the active oxidation of HCHO as shown in Figure 5. Three types of Mn tunnel structures were investigated including pyrolusite with tunnel structure of ca.  $0.23 \times 0.23 \text{ nm}^2$ , cryptomelane consisting of double edge sharing  $\text{MnO}_6$  octahedral with tunnel diameter of ca.  $0.46 \times 0.46 \text{ nm}^2$  and todorokite composed of triple chains edge-sharing  $\text{MnO}_6$  with tunnel of ca.  $0.69 \times 0.69 \text{ nm}^2$ . Experimental results indicated that cryptomelane had the highest catalytic activity achieving 100% HCHO conversion at  $140^\circ\text{C}$ . Cryptomelane possesses an effective tunnel diameter close to HCHO's dynamic diameter (0.234 nm) thereby allowing better adsorption and higher catalytic activity (55). Yu et al. (41) indicated that the micropore channel structure of nest- and urchin-like  $\text{MnO}_2$  improved their catalytic activity by allowing better adsorption of HCHO compared to that of cocoon-like  $\text{MnO}_2$  without mesopores present despite having higher specific surface area.

Tian et al. (54) also highlighted that the presence of smaller catalytic pore sizes could extend the residence of HCHO molecules in the catalyst's pores thereby improve its oxidation efficiency. Correspondingly, the work of Tian et al. (56) underscored that the pore structures of nanoparticle K-OMS-2 were readily accessible to HCHO molecules, enhancing higher adsorption and better activity compared to K-OMS-2 nanorods with similar specific surface areas. Zhang et al. (19) further highlighted that the 2D layered tunnel structure of  $\delta\text{-MnO}_2$  enhanced its activity through facilitating the adsorption and desorption of HCHO to active sites compared to other structures ( $\alpha$ -,  $\beta$ - and  $\gamma$ -  $\text{MnO}_2$ ). In another research, Chen et al. (21) stressed that catalyst's activity depends



more on its porosity and nanoplatelets crystal size than specific surface area. Mesoporous hollow  $K_xMnO_2$  nanospheres, which have smaller nanoplatelets size and specific surface area twice less than those of its corresponding mesoporous honeycomb structure, achieved higher activity in HCHO oxidation.

Wang et al. (73) showed that the structure of birnessite is such that it contains HYDROXYL groups and  $H_2O$  molecules at the interlayer surface. The presence of these molecules greatly improved its catalytic activity for HCHO removal even at room temperature. After the removal of both the hydroxyl groups and  $H_2O$  molecules at high temperature, the birnessite structure collapsed and the catalyst lost its high activity. Likewise, Sidheswaran et al. (97) indicated that the existence of  $H_2O$  molecules in interstitial voids of  $MnO_2$  based catalysts with varying composition of nsutite, cryptomelane and pyrolusite contributed to its higher catalytic activity compared to 99% pyrolusite catalyst which has smaller tunnel structure and lower  $H_2O$  molecules content in its interstitial voids.

#### 4.3 Roles of active surface oxygen in HCHO oxidation

It is reported in the literature that surface oxygen species either in the form of surface adsorbed oxygen species ( $O_2^-$ ,  $O^-$  or terminal hydroxyl (OH) group (74)) and lattice oxygen are critical to the effectiveness of the catalytic oxidation of HCHO and other intermediates into  $CO_2$  and  $H_2O$  (51,67,95). However, there is a discrepancy regarding the respective roles of each type of oxygen specie for HCHO oxidation over transition metal based catalysts. For example, Zhang et al. (19) stipulated that since HCHO oxidation was shown to conform to Mars van Krevelen mechanism, abundant lattice oxygen on the catalyst surface will lead to higher catalytic activity. They further showed that the catalytic activities of four  $MnO_2$  catalysts ( $\alpha$ ,  $\beta$ ,  $\gamma$  and  $\delta$ - $MnO_2$ ) are closely linked to their respective amount of surface lattice oxygen (relative to surface adsorbed oxygen species)

and the following order of activity was established:  $\delta$ - >  $\alpha$ - >  $\beta$ - >  $\gamma$ -  $\text{MnO}_2$ . Similarly, Tang et al. (86) indicated that the catalytic activity trend of  $\text{MnO}_x$ - $\text{CeO}_2$  composite catalysts synthesized using various methods, followed the trend of their relative lattice oxygen content. Those richer in lattice oxygen relative to surface adsorbed oxygen presented better activity.

On the other hand, surface adsorbed oxygen species were shown to be directly involved in the activation of HCHO and its subsequent oxidation into  $\text{CO}_2$  and  $\text{H}_2\text{O}$  (74,75). It was shown that the activity of layered birnesite- $\text{MnO}_2$  catalysts with surface pits corresponds to the relative amount of surface adsorbed oxygen species on the catalysts (75). The surface pits acts as vacancies for activation of molecular oxygen and or  $\text{H}_2\text{O}$  into surface adsorbed oxygen and the higher the relative amount of these species the better the catalytic activity. Wang et al. (94) contended that while surface adsorbed oxygen species participates in the oxidation reaction of HCHO, lattice oxygen species enhance their formation through its complex interaction with oxygen vacancy and molecular oxygen. Huang et al. (80) reported that the enhancement of the relative amount of surface adsorbed active oxygen species was achieved through the creation of surface defects by doping Eu on  $\text{CeO}_2$ . The created oxygen vacancies served as sites for oxygen activation into active superoxide ( $\text{O}^{2-}$ ) species which could partake in surface reaction, hence enhancing the concentration of surface adsorbed oxygen and the catalyst's activity. Similarly, surface defects created on birnesite- $\text{MnO}_2$  catalysts served as pits for activation of molecular oxygen and  $\text{H}_2\text{O}$  into surface active oxygen species, hence increasing the surface density of these species leading to higher catalytic activity (74,75). Ma et al. (51) also underscored the role of surface adsorbed oxygen ( $\text{O}^{2-}$ ,  $\text{O}^\cdot$ ) in HCHO oxidation over cobalt based catalysts. They showed that catalytic activity is closely associated to the ease with which active surface oxygen desorb from catalysts surface. They further demonstrated that catalytic activity can be improved by increasing the ease

with which surface active oxygen desorb from catalyst's surface through the incorporation of Au nanoparticles into  $\text{Co}_3\text{O}_4\text{-CeO}_2$  composite. Likewise, it was demonstrated that 3D- $\text{MnO}_2$  with abundant concentration of surface adsorbed oxygen species which easily desorb from the catalyst at lower temperature exhibited better catalytic activity compared to 2D-  $\text{MnO}_2$  with lower surface adsorbed oxygen species concentration and nano- $\text{Co}_3\text{O}_4$  with virtually no active oxygen species ( $\text{O}^{2-}$ ,  $\text{O}^-$ ) present (70).

In addition, Lu et al. (87) indicated that surface adsorbed oxygen species (hydroxyl group) and not lattice oxygen are responsible for the high activity of graphene- $\text{MnO}_2$  hybrid catalyst for HCHO oxidation. They further pointed out that the abundant relative amount of surface adsorbed hydroxyl group on the catalyst did not only improve its catalytic activity but also simplified HCHO conversion pathway by direct hydroxyl ion oxidation of formate species to  $\text{CO}_2$  without the formation of CO intermediates. It was also shown that surface adsorbed hydroxyl groups were directly involved in the room temperature oxidation of HCHO on the surface of birnessite, which led to the formation of formates and carbonates (73). Similarly, Wang et al. (18) showed that the high amount of surface adsorbed oxygen in the form of hydroxyl species were responsible for the high HCHO oxidation activity of  $\delta\text{-MnO}_2/\text{PET}$  at room temperature. Similarly, Fan et al. (67) underscored that hydroxyl species on the surface of  $\text{Co}_3\text{O}_4$  are the key active surface oxygen required for the formation of dioxymethylene (DOM) species and their subsequent conversion to formate species in HCHO oxidation process.

#### 4.4 Influence of reducibility and active metal sites on catalysts surface

The surface reducibility of catalysts plays an important role in determining their catalytic activity. It indicates the amount of reactive species on the catalyst's surface and their onset reaction temperatures (54). It could also indicate catalyst's oxygen mobility, which might cause more

oxygen adsorption and further excitement to active oxygen species which participate in the oxidation reaction (19). Tian et al. (54) indicated a correlation between reduction temperature and catalytic activity for birnessite manganese based catalysts. The established trend disclosed that the lower the catalyst's reduction temperature (higher surface reducibility), the higher its HCHO oxidative activity and vice-versa. Tang et al. (86) presented that owing to solid solution formation,  $\text{MnO}_x\text{-CeO}_2$  catalysts possessed higher surface reducibility and better catalytic activity compared to pure  $\text{MnO}_x$  and  $\text{CeO}_2$ . Furthermore, the catalysts' activity reduced as surface reducibility decreased (high reduction temperature) with increasing calcination temperature because of phase segregation. Xia et al. (69) also indicated that chromia catalysts with the highest reducibility possessed the best HCHO catalytic activity. Similar trends was also reported for HCHO oxidation over  $\text{Co}_3\text{O}_4$  catalysts (67).

The active sites present on catalyst's surface are critical and key for determining activity. The higher the concentration or availability of exposed active metal sites on catalyst's surface, the better its HCHO oxidative activity. Bai et al. (70) presented that  $\text{Co}^{3+}$  ions are the surface active state and sites of 3D- $\text{Co}_3\text{O}_4$  for HCHO oxidation. The (220) crystal plane of the catalyst is majorly composed of  $\text{Co}^{3+}$  against the  $\text{Co}^{2+}$  present on the (111) crystal plane of nano- $\text{Co}_3\text{O}_4$ , thereby making it more active and achieving complete HCHO oxidation at lower temperature. Similarly, Ma et al. (51) demonstrated that the (110) facet of 2D- $\text{Co}_3\text{O}_4$  which is mainly composed of  $\text{Co}^{3+}$  is the key active facet for effective HCHO oxidation. High activity for HCHO oxidation by 3D- $\text{MnO}_2$  was attributed to the presence of high content of  $\text{Mn}^{4+}$  active sites on the exposed (110) crystal plane surface (76). These exposed ions provided sufficient sites upon which the actual oxidation reaction takes place, thereby improving its activity. It was also shown that  $\text{Mn}^{4+}$  is the active state and site for HCHO oxidation for  $\text{MnO}_x\text{-CeO}_2$  based composite and the catalyst with

the highest amount of  $\text{Mn}^{4+}$  possessed the best activity (48,86,87). Zhang et al. (19) also highlighted that amongst their investigated catalysts ( $\alpha$ ,  $\beta$ ,  $\gamma$  and  $\delta$ - $\text{MnO}_2$ ), those with the highest content of  $\text{Mn}^{4+}$  displayed the best HCHO catalytic activity. Improving the electrochemical properties of catalysts was proven to enhance their catalytic activities. Lu et al. (87) established that the charge transport ability and interfacial electron transfer of  $\text{MnO}_2$  during  $\text{Mn}^{4+}/\text{Mn}^{3+}$  redox cycle can be enhanced by incorporating graphene into  $\text{MnO}_2$  (G-Mn hybrid), which was revealed to improve the electrical conductivity of  $\text{MnO}_2$  and decrease electron transfer resistance. In addition, it offered high specific surface area and 2D plane structure for increased exposure of metal surface active sites (100).

#### 4.5 Influence of specific surface area on HCHO catalytic activity

Catalysts' specific surface area is an important parameter affecting HCHO catalytic oxidative. High specific surface area could enhance adsorption of HCHO molecules onto the catalyst's surface and help in exposing more surface active sites, improving surface lattice defect and oxygen vacancy, thereby leading to abundant surface active oxygen species (70,78), which is a key requirement for oxidation reactions. A correlation between catalyst's surface and activity was established by Wu et al. (78) for  $\text{Co}_3\text{O}_4$  nanofibers. Activity increase was observed with increasing specific surface area and pore volume as the calcination temperature increased from room temperature to  $500^\circ\text{C}$ , above which a decline in activity was observed due to the destruction of the mesopores and the consequent decrease in specific surface area at higher temperatures. Tian et al. (36) also demonstrated that higher specific surface area greatly enhanced catalytic activity for HCHO oxidation. Nanoparticle cryptomelane catalyst, with specific surface area as high as  $206\text{ m}^2/\text{g}$  and smaller uniform mesopores exhibited higher catalytic activity than the corresponding nanorod cryptomelane catalyst with a specific surface area of  $68\text{ m}^2/\text{g}$ . The high specific surface

area and small nanoparticle sizes improved cryptomelane activity by increasing the available surface active sites and more accessible pore channels for adsorption and desorption of HCHO molecules and reaction products respectively (36). Sekine (2) showed that fine  $\text{MnO}_2$  catalysts with higher specific surface area ( $163 \text{ m}^2/\text{g}$ ) achieved higher HCHO oxidation compared to  $\text{MnO}_2$  catalysts with a specific surface area of  $61 \text{ m}^2/\text{g}$ . Similarly, Tian et al. (54) also reported that birnessite structured manganese catalysts having higher specific surface area exhibited better catalytic activities compared to those with lower specific surface areas.

However, high specific surface area does not always translate into superior catalytic activities in HCHO oxidation reactions. The activity of birnessite-type  $\text{MnO}_2$  was shown to be independent on the catalysts' specific surface area trend (74) but on the relative content of surface adsorbed oxygen species and the manganese oxidation state. The catalyst with the highest manganese vacancy had the lowest specific surface area but exhibited the best catalytic activity. Shi et al. (95) also demonstrated that the activity trend of Co-Mn oxides composite with varying Co/Mn molar ratios did not follow their specific surface area trend, and in fact the catalysts with the smallest specific surface area exhibited the best catalytic activity. Complete oxidation of HCHO was achieved at  $75^\circ\text{C}$  on Co-Mn oxides (molar ratio: 3/1) with specific surface area of  $92 \text{ m}^2/\text{g}$  while only 64% conversion was attained on Co-Mn oxides (molar ratio: 2/1) with specific surface area of  $172 \text{ m}^2/\text{g}$  at the same reaction temperature. The higher activity of Co-Mn (3/1) oxides was a result of increase in the relative amount of surface adsorbed oxygen species realized from the creation of solid solution by the incorporation of Mn into the lattice structure of  $\text{Co}_3\text{O}_4$ . Fan et al. (67) also showed that  $\text{Co}_3\text{O}_4$  catalysts with high surface content of  $\text{K}^+$ ,  $\text{CO}_3^{2-}$  and  $\text{Co}^{3+}$  exhibited better activity despite having relatively smaller specific surface area.

## 5. Effect of reaction conditions on HCHO oxidation efficiency

Reaction parameters for HCHO oxidation process such as temperature, relative humidity, reactants' space velocity and HCHO concentration play great roles in ensuring the overall effectiveness of the oxidation reaction. These parameters need to be optimized especially reaction temperature considering the potential application of the process (no harmful by-products generation), in order to realize practically effective HCHO oxidation.

### 5.1 Reaction temperature and time

Reaction temperature is critical in HCHO oxidation, and generally the efficiency of HCHO oxidation over catalyst improves with increasing temperature even though some highly active catalysts are able to achieve complete oxidation at room temperature. Most of the reported transition metal based catalysts attained complete HCHO oxidation at temperatures above 100°C (21,36,55,67,73,82) with very few below 100 °C (19,21,73,87,95,98). Figure 6 presents the conversion/removal efficiency of HCHO as a function of reaction temperatures over different catalysts. However, it does not provide a basis for comparison due to the differences in the initial HCHO concentration and feed flow rate employed in various experiments. This makes it difficult to evaluate the specific reaction rates (equation 1) (74) of variously reported catalysts for rational comparison. For static systems, experiments are normally conducted at room temperature; in which case HCHO oxidation becomes a function of time in addition to other factors catalyst based factors discussed earlier (section 4). Figure 7 presents HCHO removal efficiency over various catalysts as a function of reaction time. It can be seen in Figure 7 that long reaction time is required to achieve complete HCHO removal in static system. For proper comparison, other factors such as initial HCHO concentration and the mass of catalyst used should be taken into account.

In view of these, more investigations are required to improve the activity of transition metal based catalysts at low temperature in order to compete with noble metal based catalysts which could successfully oxidize HCHO even at room temperature (48,101).

$$\text{specific reaction rates } \left( \frac{\mu\text{mol}}{\text{m}^2 \cdot \text{min}} \right) = \frac{C_{\text{HCHO}} \div 22.4 \times F \times \eta}{S_{\text{BET}} \times m} \dots\dots\dots (1)$$

Where  $C_{\text{HCHO}}$  is the inlet HCHO concentration (ppm),  $F$  is the flow rate (ml/min),  $\eta$  is the percentage HCHO conversion ( $\text{CO}_2$  generation),  $S_{\text{BET}}$  catalysts specific surface area and  $m$  is the catalyst mass.

## 5.2 Relative humidity

Relative humidity (RH) at moderate levels influences the efficiency of HCHO oxidation, however at higher RH competitive adsorption of  $\text{H}_2\text{O}$  molecules tend to block the catalyst's active surface hence impinging activity. RH also helps in replenishing the supply of surface active hydroxyl groups which are consumed during HCHO oxidation, via the reaction of  $\text{H}_2\text{O}$  vapor and surface active oxygen ( $\text{O}_2^-$ ,  $\text{O}^-$ ) (73,102). Wang et al. (18) noted that in the presence of 50% RH,  $\text{H}_2\text{O}$  vapor react with surface active oxygen to generate enough surface hydroxyl groups to sustain HCHO oxidation reaction at RT.  $\text{H}_2\text{O}$  vapor also helps in carbonates desorption from the catalyst's surface via competitive adsorption, thereby enabling recovery of catalytic activity (73). Wang et al. (73) indicated that RH in the range of 33% to 65% enhanced HCHO removal on birnessite structured manganese at room temperature. However at higher RH (92%), catalytic activity was impacted owing to competitive adsorption of  $\text{H}_2\text{O}$  molecules on the catalyst's surface. Similar effects were observed with  $\text{MnO}_2/\text{PET}$  (18): at 0% RH significant deactivation was observed due to the formation of formate species on the catalyst's surface; however at higher RH (50%), the catalyst remained active and stable while activity significantly dropped when the RH was further



raised to 80% due to competitive adsorption of H<sub>2</sub>O molecules. This conforms to the findings of Sidheswaran et al. (97).

### 5.3 Feed flow rate and feed concentration

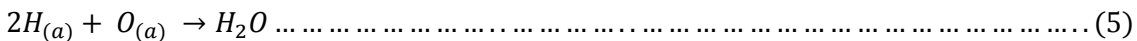
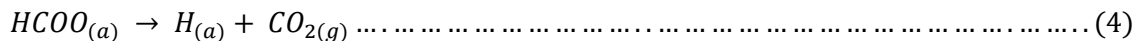
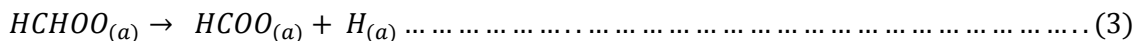
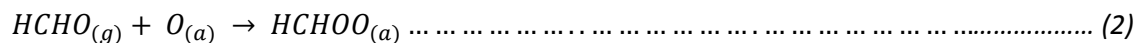
The significance of feed (reactants) flow rate in terms of gas hourly space velocity (GHSV) on catalytic oxidation of HCHO was also reported in the literature. GHSV can improve the efficiency of a fixed bed reaction system in two ways; at higher velocity, it will help to a certain extent in enhancing external mass transfer while at a lower velocity it increases the residence time of reactants in the reactor (52). It was however reported that the efficiency of HCHO oxidation reactions decreases with increasing space velocity (39,69,70,101) and vice-versa. In view of these, it could be insinuated that external mass transfer has little or no limitation on the efficiency of HCHO oxidation reaction, although an experimental evaluation on external mass transfer effect would be required.

In addition, HCHO feed concentration is another significant parameter for HCHO oxidation process. HCHO oxidation efficiency tends to decrease with an increase in the feed concentration. Chuang et al. (28) demonstrated that an increase in HCHO feed concentration led to a decrease in conversion at the same reaction temperature. Likewise, Tang et al. (48) reported that catalytic activity decreased with rise in HCHO feed concentration from 30 to 580 ppm and that the catalysts were more active and stable at lower concentration. Correspondingly, Li et al. (98) pointed out that MnO<sub>2</sub>/AC completely lost its activity when exposed to 5 mg/m<sup>3</sup> HCHO feed concentration in 32 hrs, compared to its sustained HCHO oxidation efficiency of up to 70% for 80 hrs under a HCHO feed concentration of 0.5 mg/m<sup>3</sup>.

## 6. Reaction mechanism of catalytic oxidation of HCHO

Understanding the reaction mechanism of HCHO oxidation over transition metal based catalysts is vital for the development of catalysts with high efficiency, low cost and good stability. Different catalysts for HCHO oxidation may exhibit varying reaction mechanisms because different intermediate species could be formed with various active oxygen species and surface active sites (4). Oxidation reaction of HCHO over some transition metals based catalysts were shown to conform to Mars-van Krevelen mechanism (18,19,97). In this mechanism, reaction proceeds via a two-stage redox reaction with an assumption of constant surface oxygen. The catalyst's surface is first oxidized by gas phase molecular oxygen to form surface adsorbed oxygen species which subsequently reduces the pollutant (52).

Sekine (2) proposed that HCHO oxidation on metal oxides catalysts proceeds first by adsorption on the catalyst's surface followed by decomposition through the formation of formate intermediates on the surface, then the intermediates are subsequently decomposed to H<sub>2</sub>O and CO<sub>2</sub> as presented in equations (2-5) where *g* and *a* indicate gaseous phase and adsorbed species, respectively.



Tang et al. (86) indicated the oxidation of HCHO over MnO<sub>x</sub>-CeO<sub>2</sub> catalyst was attained through the effective transfer of oxygen species from CeO<sub>2</sub> oxygen reservoir to MnO<sub>2</sub> active state. This synergy is achieved through the effective activation of feed molecular oxygen and the transfer of

the activated oxygen to replace the released active oxygen species from  $\text{MnO}_2$  which participated in HCHO oxidation through a series of redox cycles involving  $\text{Mn}^{4+}/\text{Mn}^{3+}$  and  $\text{Ce}^{4+}/\text{Ce}^{3+}$  (48,86) as shown in Figure 8.

Wang et al. (73) proposed three-step mechanism for HCHO oxidation on birnessite structured manganese catalyst at room temperature as presented in Figure 9. The reaction first proceeds through H-bond between HCHO molecules and birnessite bonded  $\text{H}_2\text{O}$  molecules. The adsorbed molecules are then oxidized to formate and carbonates by structural hydroxyl species. Subsequently, the consumed hydroxyl ions are replaced through the reaction between surface active oxygen and  $\text{H}_2\text{O}$  molecules. An oxygen vacancy is then formed on the site of the consumed surface active oxygen species, which further acts as a site for molecular oxygen activation to active species for continuous reaction (74). Wang et al. (68) reported that only hydrocarbonate species were observed on the surface of 3D-Co-Mn catalysts with no obvious formation of formate species, probably due to the fast conversion rate of formate to hydrocarbonates on the catalyst's surface as suggested by the authors. The hydrocarbonate species were totally decomposed at  $70^\circ\text{C}$  as reported by Shi et al. (95) for Co-Mn.

Shi et al. (95) indicated that the mechanism of HCHO oxidation over Co-Mn oxides proceeds via the formation of DOM and formate species as intermediates. During adsorption process, HCHO is immediately converted to DOM as no HCHO molecules were observed on the catalyst surface at room temperature. The active DOM species react with surface adsorbed oxygen species to form formate species and part of them are further oxidized to hydrocarbonates. At higher temperature ( $50^\circ\text{C}$ ), further oxidation of formate and degradation of hydrocarbonate species occur. At the complete oxidation temperature of HCHO ( $75^\circ\text{C}$ ), only adsorbed  $\text{H}_2\text{O}$  molecules were observed, indicating complete oxidation of all the intermediate species. Hence, formate oxidation and

hydrocarbonate decomposition are considered as the rate-limiting steps for HCHO oxidation over Co-Mn oxides catalyst.

A reaction mechanism for 2D ordered mesoporous  $\text{Co}_3\text{O}_4$ ,  $\text{Au}/\text{Co}_3\text{O}_4$  and  $\text{Au}/\text{Co}_3\text{O}_4\text{-CeO}_2$  at room temperature had been proposed by Ma et al. (51) as depicted in Figure 10. In this mechanism, formate species are first generated by the nucleophilic attack on the C-H in HCHO by surface active oxygen on the (110) facet of  $\text{Co}_3\text{O}_4$  (with  $\text{Co}^{3+}$  as the active state). The formate species are further oxidized to bicarbonates by surface active oxygen species. Carbonic acid species are then generated by the reaction of the bicarbonates and  $\text{H}^+$ , which are subsequently decomposed to  $\text{CO}_2$ . In contrast, Fan et al. (67) indicated that hydroxyl groups were responsible for the immediate oxidation of HCHO on the surface of  $\text{Co}_3\text{O}_4$  and that DOM and formate species were observed as the intermediates during the adsorption of HCHO on the catalyst's surface as previously reported (95). However, the behavior of the catalysts at elevated temperature in the presence of  $\text{O}_2$  was influenced by the existence of  $\text{K}^+$  ions on the catalyst's surface. In the presence of  $\text{K}^+$  ions, DOM species generated during the adsorption process are converted to formate species and formate oxidation to bicarbonates becomes the key reaction step. It was proposed that hydroxyl groups were generated from surface hydrolysis of  $\text{K}_2\text{CO}_3$  and got consumed during the reaction. The consumed hydroxyl groups were replenished by the  $\text{H}_2\text{O}$  molecules generated thus  $\text{K}_2\text{CO}_3$  surface hydrolysis was sustained and the reaction was accelerated. On the other hand, in the absence of  $\text{K}_2\text{CO}_3$  at elevated temperature ( $80^\circ\text{C}$ ) only few DOM species could be converted to formate species due to the lack of hydroxyl groups on the surface of  $\text{Co}_3\text{O}_4$ , thus formate decomposition to carbonates and bicarbonates became the key reaction step at  $\geq 80^\circ\text{C}$ . Here it could be observed that the existence of  $\text{K}^+$  on the surface of  $\text{Co}_3\text{O}_4$  changed the reaction path from formate decomposition to formate oxidation and continued supply of surface hydroxyl group necessary for

the oxidation reaction was sustained by  $\text{K}_2\text{CO}_3$  surface hydrolysis thus promoting HCHO oxidation. Similar promotion effects of  $\text{K}^+$  was observed for  $\text{Ag}/\text{Co}_3\text{O}_4$  (46),  $\text{Na}^+$  for ceramic honeycombs (103) and  $\text{Na}^+$  for  $\text{Pd}/\text{TiO}_2$  (59).

Lu et al. (87) proposed a reaction pathway for HCHO over graphene- $\text{MnO}_2$  hybrid catalysts. In this mechanism, HCHO is first oxidized to form formate intermediates while molecular oxygen is activated and transferred to active Mn sites through  $\text{Mn}^{4+}/\text{Mn}^{3+}$  redox cycle. Graphene being an electrical conductor reduces electron transfer resistance and enhances the rate of charge transfer between  $\text{Mn}^{4+}$  and  $\text{Mn}^{3+}$ , thereby improving the overall efficiency of the process. Thereafter, due to the abundant amount of surface hydroxyl groups on the hybrid catalyst, formate species were directly converted to  $\text{CO}_2$  and  $\text{H}_2\text{O}$ , while the consumed hydroxyl ions were regenerated by the produced  $\text{H}_2\text{O}$  molecules as reported by other authors (67).

The reaction mechanism of HCHO catalytic oxidation is intricate and varies with the type and amount of surface active oxygen or hydroxyl species present. But generally, formate species are key intermediates present on almost all transition metal based catalysts. Other species such as DOM and hydrocarbonates are also reported as intermediates for HCHO oxidation. However, the reported pathways for HCHO decomposition varied in the literature. In some mechanisms DOM species are first generated followed by their conversion to formate intermediates, which are subsequently oxidized to hydrocarbonates and finally  $\text{CO}_2$  and  $\text{H}_2\text{O}$  molecules are generated by hydrocarbonate decomposition. In other mechanisms, no DOM species are observed and formates are directly oxidized to  $\text{CO}_2$  and  $\text{H}_2\text{O}$  especially in the presence of high amount of surface hydroxyl groups (67,87). The reaction mechanism of transition metal based catalysts for HCHO oxidation is minimally reported in the literature. This prompts the need for further elaborate investigation into the mechanism on various active transition metals especially as it relates to the surface

properties of these catalysts, and the specific role of hydroxyl and oxygen species and the promotional effects of alkali metals ( $\text{Na}^+$ ,  $\text{K}^+$ ) on the overall efficiency of the reaction. This will provide more information and offer the basis for the design of yet more active and cost-effective catalysts for practical application.

## **7. Conclusions and outlook**

Formaldehyde is one of the most harmful indoor air pollutants as it has adverse effects on human health due to its toxicity and carcinogenicity. Techniques such as adsorption, photo-catalytic oxidation and catalytic oxidation have been used in HCHO removal. Adsorption removal is limited by the adsorption capacity of the adsorbents deployed and the hazard of HCHO desorption during regeneration while photo-catalytic oxidation produces hazardous by-products. Catalytic oxidation offsets these drawbacks and can achieve complete conversion of HCHO into  $\text{CO}_2$  and  $\text{H}_2\text{O}$  molecules without the formation of hazardous by-products.

Noble metal based catalysts exhibit excellent low and even room temperature HCHO oxidation capabilities but their practical application is restricted by their cost and availability. Recent investigations focus on the use of relatively cheap and abundant transition metals oxides and improving their low temperature performance. More attention has mainly been focused on the improvement and exploitation of various structures and morphologies of manganese oxide catalysts due to its high activity yet with little attention on other transition metal catalysts. As such, more investigation needs to be done on the improvement of morphological structures, textural and redox properties of these materials.

For practical air purification application in air purifiers or building HVAC systems, substrate materials with low air resistance and pressure drop are required to immobilize catalysts to avoid

829 dust contamination and catalysts leaching into treated air stream. However, only a few substrate  
830 materials have been reported in the literature and hence the need for further evaluation of more  
831 materials to understand their interactions with the catalysts and effect on activity for pragmatic air  
832 purification process. In addition to the development of these materials, they need to be tested under  
833 real indoor environmental conditions in air purifiers to evaluate the effects of system conditions  
834 such as face velocity, dust particle contamination and particle leaching on the efficiency and  
835 stability of the catalysts.

836 No single property is decisive for catalytic performance of transition metal oxides for complete  
837 oxidation of HCHO but a combination of several factors which include specific surface area, metal  
838 oxidation state, adsorbed and surface oxygen species, structure and morphology of the catalyst.  
839 Improvement of the morphological structures of transition metal based catalysts relative to their  
840 conventional bulk counterparts enhances their catalytic activity through improvement of specific  
841 surface area, mesoporosity and exposure of surface active metals and oxygen species. The tunnel  
842 structure of catalysts enhances the rate of adsorption of HCHO onto the active sites for  
843 decomposition and the rate of product desorption from the sites to make them available for the  
844 next molecules. This is particularly promoted when the catalyst's effective diameter is close to the  
845 dynamic diameter of HCHO (55). Oxidation state of metals in the catalyst is also vital for  
846 determining activity and higher oxidation states seem to be more active;  $\text{Mn}^{4+}$  in the case of  
847 manganese and  $\text{Co}^{3+}$  in the case of cobalt were identified to be the most active states for HCHO  
848 activation. Several methods have been proposed for improving the oxidation state of metal oxides  
849 which include modified synthesis, controlling calcination temperature and the relative molar ratio  
850 of component elements, to maintain solid solution stability in the case of composite catalysts (86).

The use of hard template materials has been proven effective in providing the plane structure for improved exposure of more surface active sites and enhanced access to these sites.

Active surface oxygen and hydroxyl species directly participate in oxidizing HCHO molecules and all other intermediate species into CO<sub>2</sub> and H<sub>2</sub>O. The higher the concentration of these active materials on the catalyst's surface the better its HCHO oxidative activity. The availability of surface active oxygen species and the rate of molecular oxygen activation could be enhanced by the formation of surface vacancy using dopants and formation of solid solution composites with oxygen carrier materials. Recently reported works (80,81) indicated that creating oxygen surface vacancy using dopants increases the activation rate of molecular oxygen to more active and reactive oxygen species thereby providing more abundant oxygen species for HCHO oxidation. However not much has been reported on surface vacancy creation and surface modification using dopants on transition metal based catalyst for HCHO oxidation, thereby prompting the need for further exploration. The use of oxygen carrier materials for composite formation on the other hand improves the transfer rate of active oxygen from the rich oxygen sources of the carrier to the active metal sites in a complete redox cycle. The formation of solid solution within the solubility limit of the composite is critical to achieving synergistic effects either through oxygen transfer or oxygen vacancy creation, above which phase segregation occurs and synergy is lost. Most of the reported composites in the literature for HCHO oxidation focus on the use of CeO<sub>2</sub> as composite material with little or no attention to other oxygen carriers.

Furthermore, enhancing the electrical conductivity of catalyst through the formation of hybrids or composites with electrically conducting materials such as graphene (87) was shown to greatly improve catalytic activity at low temperature. The hybrid system exposed more Mn<sup>4+</sup> active sites, enhanced charge transport during Mn redox cycle and offered higher content of surface hydroxyl



species, which eases HCHO oxidation and improves the catalyst's activity at low temperature. However, very few studies have been reported for catalyst's electrical conductivity enhancement using conductor materials for HCHO oxidation. Hence further investigation into the influence of dopants and other conductor materials on the activity of transition metals based catalysts for improved low temperature HCHO oxidation will be desirable. In addition to catalytic properties, reaction parameters such as reaction temperature, relative humidity, space velocity and HCHO feed concentration also affect the overall efficiency of HCHO oxidation. Relative humidity at moderate levels helps in enhancing the availability of surface active hydroxyl groups via the reaction of H<sub>2</sub>O vapor and surface active oxygen but becomes detrimental at higher levels.

The reaction mechanism of HCHO is complex and depends on the type of catalysts, the oxidation state and amount of active metals and the nature of surface active oxygen (adsorbed and or lattice) present. Although further research is required to ascertain the respective role of each in HCHO oxidation. Only a few mechanisms were reported for transition metal catalysts, as such further investigation is required into the reaction mechanism especially as it relates to the catalyst's surface properties and the role of surface active oxygen or hydroxyl species. But generally, formate species, DOM and hydrocarbonates are the identified intermediates for HCHO oxidation on transition metal based catalysts. However, the reported pathways for HCHO decomposition varied in the literature. In some mechanisms DOM species are first generated followed by DOM conversion to formate intermediates, which are subsequently oxidized to hydrocarbonates and finally CO<sub>2</sub> and H<sub>2</sub>O molecules are generated by hydrocarbonate decomposition. In other mechanisms, no DOM species are observed and formates are directly oxidized to CO<sub>2</sub> and H<sub>2</sub>O molecules without the formation of hydrocarbonates especially in the presence of high amount of surface hydroxyl groups.

897    **Acronyms**

898	1D	One Dimensional
899	2D	Two Dimensional
900	3D	Three Dimensional
901	3DOM	Three Dimensional Ordered Macroporous
902	AC	Activated Carbon
903	CTAB	Cetyltrimethylammonium Bromide
904	DOM	Dioxymethylene
905	GHSV	Gas Hourly Space Velocity
906	HCHO	Formaldehyde
907	HVAC	Heating Ventilation and Air Conditioning
908	IARC	International Agency for Research on Cancer
909	KIT-6	Korea Advanced Institute of Science and Technology-6
910	K-OMS-2	Potassium-Octahedral Molecular Seive-2
911	PET	Polyethylene Terephthalate
912	R	Specific Reaction Rate
913	Redox	Reduction-Oxidation
914	RH	Relative humidity
915	SBA-15	Santa Barbara Amorphous-15
916	TOF	Turnover Frequency
917	VOC	Volatile Organic Compounds
918	WHO	World Health Organization

919    **Acknowledgement**

920    This work was carried out at the International Doctoral Innovation Centre (IDIC). The authors  
921    acknowledge the financial support from the International Doctoral Innovation Centre, Ningbo  
922    Education Bureau, Ningbo Science and Technology Bureau, China's MOST and The University

923 of Nottingham. This work is also partially supported by Zhejiang Provincial Applied Research  
924 Program for Commonweal Technology (2015C33011), EPSRC grant EP/L016362/1, Natural  
925 Science Foundation of China (41303091) and Strategic Priority Research Program (B) of the  
926 Chinese Academy of Sciences (XDB05020403).

## References

- (1) Maddalena, R.; Russell, M.; Sullivan, D.P.; Apte, M.G. Formaldehyde and Other Volatile Organic Chemical Emissions in Four FEMA Temporary Housing Units. *Environ. Sci. Technol.* **2009**, *43* (15), 5626-5632.
- (2) Sekine, Y. Oxidative decomposition of formaldehyde by metal oxides at room temperature. *Atmos. Environ.* **2002**, *36* (35), 5543-5547.
- (3) Salthammer, T.; Mentese, S.; Marutzky, R. Formaldehyde in the Indoor Environment. *Chem. Rev.* **2010**, *110* (4), 2536-2572.
- (4) Bai, B.; Qiao, Q.; Li, J.; Hao, J. Progress in research on catalysts for catalytic oxidation of formaldehyde. *Chin. J. Catal.* **2016**, *37* (1), 102-122.
- (5) Sekine, Y.; Nishimura, A. Removal of formaldehyde from indoor air by passive type air-cleaning materials. *Atmos. Environ.* **2001**, *35* (11), 2001-2007.
- (6) International Agency for Cancer Research (IACR) working group on the identification of Carcinogenic Risks to Humans. *Formaldehyde, 2-Butoxyethanol and 1-tert-Butoxypropan-2-ol*. WHO; Lyon France, 2006; volume 88.
- (7) World Health Organization. *WHO guidelines for indoor air quality: selected pollutants*; WHO: Copenhagen, 2010.
- (8) Le, Y.; Guo, D.; Cheng, B.; Yu, J. Bio-template-assisted synthesis of hierarchically hollow SiO<sub>2</sub> microtubes and their enhanced formaldehyde adsorption performance. *Appl. Surf. Sci.* **2013**, *274*, 110-116.
- (9) Chen, D.; Qu, Z.; Sun, Y.; Wang, Y. Adsorption-desorption behavior of gaseous formaldehyde on different porous Al<sub>2</sub>O<sub>3</sub> materials. *Colloids Surf., A* **2014**, *441* 433-440.
- (10) Ma, C.; Li, X.; Zhu, T. Removal of low-concentration formaldehyde in air by adsorption on activated carbon modified by hexamethylene diamine. *Carbon* **2011**, *49* (8), 2873-2875.
- (11) Rezaee, A.; Rangkooy, H.; Jonidi-Jafari, A.; Khavanin, A. Surface modification of bone char for removal of formaldehyde from air. *Appl. Surf. Sci.* **2013**, *286*, 235-239.
- (12) Lu, Y.; Wang, D.; Ma, C.; Yang, H. The effect of activated carbon adsorption on the photocatalytic removal of formaldehyde. *Build. Environ.* **2010**, *45* (3), 615-621.
- (13) Tong, H.; Zhao, L.; Li, D.; Zhang, X. N, Fe and WO<sub>3</sub> modified TiO<sub>2</sub> for degradation of formaldehyde. *J. Alloys Compd.* **2011**, *509* (22), 6408-6413.
- (14) Fu, P.; Zhang, P.; Li, J. Photocatalytic degradation of low concentration formaldehyde and simultaneous elimination of ozone by-product using palladium modified TiO<sub>2</sub> films under UV 254+ 185nm irradiation. *Appl. Catal., B* **2011**, *105* (1), 220-228.
- (15) Liang, W.; Li, J.; Jin, Y. Photo-catalytic degradation of gaseous formaldehyde by TiO<sub>2</sub>/UV, Ag/TiO<sub>2</sub>/UV and Ce/TiO<sub>2</sub>/UV. *Build. Environ.* **2012**, *51*, 345-350.

- (16) Ghosh, J.P.; Sui, R.; Langford, C.H.; Achari, G.; Berlinguette, C.P. A comparison of several nanoscale photocatalysts in the degradation of a common pollutant using LEDs and conventional UV light. *Water Res.* **2009**, *43* (18), 4499-4506.
- (17) Shie, J.L.; Lee, C.H.; Chiou, C.S.; Chang, C.T.; Chang, C.C.; Chang, C.Y. Photodegradation kinetics of formaldehyde using light sources of UVA, UVC and UVLED in the presence of composed silver titanium oxide photocatalyst. *J. Hazard. Mater.* **2008**, *155* (1), 164-172.
- (18) Wang, J.; Yunus, R.; Li, J.; Li, P.; Zhang, P.; Kim, J. In situ synthesis of manganese oxides on polyester fiber for formaldehyde decomposition at room temperature. *Appl. Surf. Sci.* **2015**, *357*, 787-794.
- (19) Zhang, J.; Li, Y.; Wang, L.; Zhang, C.; He, H. Catalytic oxidation of formaldehyde over manganese oxides with different crystal structures. *Catal. Sci. Technol.* **2015**, *5* (4), 2305-2313.
- (20) Luengas, A.; Barona, A.; Hort, C.; Gallastegui, G.; Platel, V.; Elias, A. A review of indoor air treatment technologies. *Rev. Environ. Sci. Bio/Technol.* **2015**, *14* (3), 499-522.
- (21) Chen, H.; He, J.; Zhang, C.; He, H. Self-assembly of novel mesoporous manganese oxide nanostructures and their application in oxidative decomposition of formaldehyde. *J. Phys. Chem. C* **2007**, *111* (49), 18033-18038.
- (22) Zhang, C.; He, H. A comparative study of TiO<sub>2</sub> supported noble metal catalysts for the oxidation of formaldehyde at room temperature. *Catal. Today* **2007**, *126* (3), 345-350.
- (23) Zhang, C.; Liu, F.; Zhai, Y.; Ariga, H.; Yi, N.; Liu, Y.; Asakura, K.; Flytzani - Stephanopoulos, M.; He, H. Alkali- Metal- Promoted Pt/TiO<sub>2</sub> Opens a More Efficient Pathway to Formaldehyde Oxidation at Ambient Temperatures. *Angew. Chem., Int. Ed.* **2012**, *51* (38), 9628-9632.
- (24) Huang, H.; Leung, D.Y. Complete elimination of indoor formaldehyde over supported Pt catalysts with extremely low Pt content at ambient temperature. *J. Catal.* **2011**, *280* (1), 60-67.
- (25) Kim, S.S.; Park, K.H.; Hong, S.C. A study on HCHO oxidation characteristics at room temperature using a Pt/TiO<sub>2</sub> catalyst. *Appl. Catal., A* **2011**, *398* (1), 96-103.
- (26) Yan, Z.; Xu, Z.; Yu, J.; Jaroniec, M. Enhanced formaldehyde oxidation on CeO<sub>2</sub>/AlOOH-supported Pt catalyst at room temperature. *Appl. Catal., B* **2016**, *199*, 458-465.
- (27) Nie, L.; Jiaguo, Y.; Xinyang, L.; Bei, C.; Gang, L.; Mietek, J. Enhanced performance of NaOH-modified Pt/TiO<sub>2</sub> toward room temperature selective oxidation of formaldehyde. *Environ. Sci. Technol.* **2013**, *47* (6), 2777-2783.
- (28) Chuang, K.T.; Zhou, B.; Tong, S. Kinetics and Mechanism of Catalytic Oxidation of Formaldehyde over Hydrophobic Catalysts. *Ind. Eng. Chem. Res.* **1994**, *33* (7), 1680-1686.
- (29) An, N.; Zhang, W.; Yuan, X.; Pan, B.; Liu, G.; Jia, M.; Yan, W.; Zhang, W. Catalytic oxidation of formaldehyde over different silica supported platinum catalysts. *Chem. Eng. J. (Amsterdam, Neth.)* **2013**, *215*, 1-6.

- (30) Peng, J.; Wang, S. Performance and characterization of supported metal catalysts for complete oxidation of formaldehyde at low temperatures. *Appl. Catal., B* **2007**, *73* (3), 282.
- (31) Park, S.J.; Bae, I.; Nam, I.S.; Cho, B.K.; Jung, S.M.; Lee, J.H. Oxidation of formaldehyde over Pd/Beta catalyst. *Chem. Eng. J. (Amsterdam, Neth.)* **2012**, *195*, 392-402.
- (32) de la Peña O'Shea, V. A.; Alvarex-Galvan, M.C; Fierro, J.L.; Arias, P. L. Influence of feed composition on the activity of Mn and PdMn/Al<sub>2</sub>O<sub>3</sub> catalysts for combustion of formaldehyde/methanol. *Appl. Catal., B* **2005**, *57* (3), 191-199.
- (33) Huang, H.; Leung, D.Y. Complete Oxidation of Formaldehyde at Room Temperature Using TiO<sub>2</sub> Supported Metallic Pd Nanoparticles. *ACS Catal.* **2011**, *1* (4), 348-354.
- (34) Mao, C.F.; Vannice, M. A. Formaldehyde Oxidation Over Ag Catalysts. *J. Catal.* **1995**, *154* (2), 230-244.
- (35) Qu, Z.; Shen, S.; Chen, D.; Wang, Y. Highly active Ag/SBA-15 catalyst using post-grafting method for formaldehyde oxidation. *J. Mol. Catal. A: Chem.* **2012**, *356*, 171-177.
- (36) Tian, H.; He, J.; Liu, L.; Wang, D. Effects of textural parameters and noble metal loading on the catalytic activity of cryptomelane-type manganese oxides for formaldehyde oxidation. *Ceram. Int.* **2013**, *129* (1), 315-321.
- (37) Li, H. F.; Zhang, N.; Chen, P.; Luo, M. F.; Lu, J. Q. High surface area Au/CeO<sub>2</sub> catalysts for low temperature formaldehyde oxidation. *Appl. Catal., B* **2011**, *110*, 279-285.
- (38) Imamura, S.; Uchihori, D.; Utani, K.; Ito, T. Oxidative decomposition of formaldehyde on silver-cerium composite oxide catalyst *Catal. Lett.* **1994**, *24* (3-4), 377-384.
- (39) An, N.; Yu, Q.; Liu, G.; Li, S.; Jia, M.; Zhang, W. Complete oxidation of formaldehyde at ambient temperature over supported Pt/Fe<sub>2</sub>O<sub>3</sub> catalysts prepared by colloid-deposition method. *J. Hazard. Mater.* **2011**, *186* (2), 1392-1397.
- (40) Shen, Y.; Yang, X.; Wang, Y.; Zhang, Y.; Zhu, H.; Gao, L.; Jia, M. The states of gold species in CeO<sub>2</sub> supported gold catalyst for formaldehyde oxidation. *Appl. Catal., B* **2008**, *79* (2), 142-148.
- (41) Yu, X.; He, J.; Wang, D.; Hu, Y.; Tian, H.; He, Z. Facile Controlled Synthesis of Pt/MnO<sub>2</sub> Nanostructured Catalysts and Their Catalytic Performance for Oxidative Decomposition of Formaldehyde. *J. Phys. Chem. C* **2011**, *116* (1), 851-860.
- (42) Hu, P.; Amghouz, Z.; Huang, Z.; Xu, F.; Chen, Y.; Tang, X. Surface-Confined Atomic Silver Centers Catalyzing Formaldehyde Oxidation. *Environ. Sci. Technol.* **2015**, *49* (4), 2384-2390.
- (43) Bai, B.; Qiao, Q.; Arandiyana, H.; Li, J.; Hao, J. Three-Dimensional Ordered Mesoporous MnO<sub>2</sub>-Supported Ag Nanoparticles for Catalytic Removal of Formaldehyde. *Environ. Sci. Technol.* **2016**, *50* (5), 2635-2640.
- (44) Zhang, J.; Jin, Y.; Li, C.; Shen, Y.; Han, L.; Hu, Z.; Di, X.; Liu, Z. Creation of three-dimensionally ordered macroporous Au/CeO<sub>2</sub> catalysts with controlled pore sizes and their enhanced catalytic performance for formaldehyde oxidation. *Appl. Catal., B* **2009**, *91* (1), 11-20.

- (45) Wang, R.; Li, J. OMS-2 Catalysts For Formaldehyde Oxidation: Effects of Ce And Pt on Structure And Performance of the Catalysts. *Catal. Lett.* **2009**, *131* (3-4), 500-505.
- (46) Bai, B.; Li, J. Positive Effects of K<sup>+</sup> Ions on Three-Dimensional Mesoporous Ag/Co<sub>3</sub>O<sub>4</sub> Catalyst For HCHO Oxidation. *ACS Catal.* **2014**, *4* (8), 2753-2762.
- (47) Ma, L.; Wang, D.; Li, J.; Bai, B.; Fu, L.; Li, Y. Ag/CeO<sub>2</sub> nanospheres: Efficient catalysts for formaldehyde oxidation. *Appl. Catal., B* **2014**, *148*, 36-43.
- (48) Tang, X.; Chen, J.; Huang, X.; Xu, Y.; Shen, W. Pt/MnO<sub>x</sub>-CeO<sub>2</sub> catalysts for the complete oxidation of formaldehyde at ambient temperature. *Appl. Catal., B* **2008**, *81* (1), 115-121.
- (49) Tang, X.; Chen, J.; Li, Y.; Li, Y.; Xu, Y.; Shen, W. Complete oxidation of formaldehyde over Ag/MnO<sub>x</sub>-CeO<sub>2</sub> catalysts. *Chem. Eng. J. (Amsterdam, Neth.)* **2006**, *118* (1), 119-125.
- (50) Liu, B.; Liu, Y.; Li, C.; Hu, W.; Jing, P.; Wang, Q.; Zhang, J. Three-dimensionally ordered macroporous Au/CeO<sub>2</sub>-Co<sub>3</sub>O<sub>4</sub> catalysts with nanoporous walls for enhanced catalytic oxidation of formaldehyde. *Appl. Catal., B* **2012**, *127*, 47-58.
- (51) Ma, C.; Wang, D.; Xue, W.; Dou, B.; Wang, H.; Hao, Z. Investigation of Formaldehyde Oxidation over Co<sub>3</sub>O<sub>4</sub>-CeO<sub>2</sub> and Au/Co<sub>3</sub>O<sub>4</sub>-CeO<sub>2</sub> Catalysts at Room Temperature: Effective Removal and Determination of Reaction Mechanism. *Environ. Sci. Technol.* **2011**, *45* (8), 3628-3634.
- (52) Pei, J.; Zhang, J.S. Critical review of catalytic oxidization and chemisorption methods for indoor formaldehyde removal. *HVACR Res.* **2011**, *17* (4), 476-503.
- (53) Quiroz, J.; Giraudon, J.M.; Gervasini, A.; Dujardin, C.; Lancelot, C.; Trentesaux, M.; Lamonier, J.F. Total Oxidation of Formaldehyde over MnO<sub>x</sub>-CeO<sub>2</sub> Catalysts: The Effect of Acid Treatment. *ACS Catal.* **2015**, *5* (4), 2260-2269.
- (54) Tian, H.; He, J.; Liu, L.; Wang, D.; Hao, Z.; Ma, C. Highly active manganese oxide catalysts for low-temperature oxidation of formaldehyde. *Microporous Mesoporous Mater.* **2012**, *151*, 397-402.
- (55) Chen, T.; Dou, H.; Li, X.; Tang, X.; Li, J.; Hao, J. Tunnel structure effect of manganese oxides in complete oxidation of formaldehyde. *Microporous Mesoporous Mater.* **2009**, *122* (1), 270-274.
- (56) Tian, H.; He, J.; Zhang, X.; Zhou, L.; Wang, D. Facile synthesis of porous manganese oxide K-OMS-2 materials and their catalytic activity for formaldehyde oxidation. *Microporous Mesoporous Mater.* **2011**, *138* (1), 118-122.
- (57) Tasbihi, M.; Bendyna, J. K.; Notten, P. H. A Short Review on Photocatalytic Degradation of Formaldehyde. *J. Nanosci. Nanotechnol.* **2015**, *15* (9), 6386-6396.
- (58) Chen, B.B.; Shi, C.; Crocker, M.; Wang, Y.; Zhu, A.M. Catalytic removal of formaldehyde at room temperature over supported gold catalysts. *Appl. Catal., B* **2013**, *132*, 245-255.
- (59) Zhang, C.; Li, Y.; Wang, Y.; He, H. Sodium-Promoted Pd/TiO<sub>2</sub> for Catalytic Oxidation of Formaldehyde at Ambient Temperature. *Environ. Sci. Technol.* **2014**, *48* (10), 5816-5822.

- (60) Xu, Z.; Yu, J.; Jaroniec, M. Efficient catalytic removal of formaldehyde at room temperature using AlOOH nanoflakes with deposited Pt. *Appl. Catal., B* **2015**, *163*, 306-312.
- (61) Li, D.; Yang, G.; Li, P.; Wang, J.; Zhang, P. Promotion of Formaldehyde Oxidation over Ag Catalyst by Fe Doped MnO<sub>x</sub> Support at Room Temperature. *Catal. Today* **2016**, *277*, 257-265.
- (62) Zhang, Y.; Shen, Y.; Yang, X.; Sheng, S.; Wang, T.; Adebajo, M. F.; Zhu, H. Gold catalysts supported on the mesoporous nanoparticles composited of zirconia and silicate for oxidation of formaldehyde. *J. Mol. Catal. A: Chem.* **2010**, *316*, 100-105.
- (63) Li, C.; Shen, Y.; Jia, M.; Sheng, S.; Adebajo, M. O.; Zhu, H. Catalytic combustion of formaldehyde on gold/iron-oxide catalysts. *Catal. Commun.* **2008**, *9* (3), 355-361.
- (64) Xu, Q.; Lei, W.; Li, X.; Qi, X.; Yu, J.; Liu, G.; Wang, J.; Zhang, P. Efficient Removal of Formaldehyde by Nanosized Gold on Well-Defined CeO<sub>2</sub> Nanorods at Room Temperature. *Environ. Sci. Technol.* **2014**, *48* (16), 9702-9708.
- (65) Chen, H.; Tang, M.; Rui, Z.; Ji, H. MnO<sub>2</sub> Promoted TiO<sub>2</sub> Nanotube Array Supported Pt Catalyst for Formaldehyde Oxidation with Enhanced Efficiency. *Ind. Eng. Chem. Res.* **2015**, *54* (36), 8900-8907.
- (66) Chen, Y.; He, J.; Tian, H.; Wang, D.; Yang, Q. Enhanced formaldehyde oxidation on Pt/MnO<sub>2</sub> catalysts modified with alkali metal salts. *J. Colloid Interface Sci.* **2014**, *428*, 1-7.
- (67) Fan, Z.; Zhang, Z.; Fang, W.; Yao, X.; Zou, G.; Shangguan, W. Low-temperature catalytic oxidation of formaldehyde over Co<sub>3</sub>O<sub>4</sub> catalysts prepared using various precipitants. *Chin. J. Catal.* **2016**, *37* (6), 947-954.
- (68) Wang, Y.; Zhu, A.; Chen, B.; Crocker, M.; Shi, C. Three-dimensional ordered mesoporous Co-Mn oxide: A highly active catalyst for "storage-oxidation" cycling for the removal of formaldehyde. *Catal. Commun.* **2013**, *36*, 52.
- (69) Xia, Y.; Dai, H.; Zhang, L.; Deng, J.; He, H.; Au, C.T. Ultrasound-assisted nanocasting fabrication and excellent catalytic performance of three-dimensionally ordered mesoporous chromia for the combustion of formaldehyde, acetone and methanol. *Appl. Catal., B* **2010**, *100* (1), 229-237.
- (70) Bai, B.; Arandiyani, H.; Li, J. Comparison of the performance for oxidation of formaldehyde on nano-Co<sub>3</sub>O<sub>4</sub>, 2D-Co<sub>3</sub>O<sub>4</sub>, and 3D-Co<sub>3</sub>O<sub>4</sub> catalysts. *Appl. Catal., B* **2013**, *142*, 677-683.
- (71) Dai, Z.; Yu, X.; Huang, C.; Li, M.; Su, J.; Guo, Y.; Xu, H.; Ke, Q. Nanocrystalline MnO<sub>2</sub> on an activated carbon fiber for catalytic formaldehyde removal. *RSC Adv.* **2016**, *6* (99), 97022-97029.
- (72) Feng, Q.; Kanoh, H.; Ooi, K. Manganese oxide porous crystals. *J. Mater. Chem.* **1999**, *9* (2), 319-333.
- (73) Wang, J.; Zhang, P.; Li, J.; Jiang, C.; Yunus, R.; Kim, J. Room-Temperature Oxidation of Formaldehyde by Layered Manganese Oxide: Effect of Water. *Environ. Sci. Technol.* **2015**, *49* (20), 12372-12379.



- (74) Wang, J.; Li, J.; Jiang, C.; Zhou, P.; Zhang, P.; Yu, J. The effect of manganese vacancy in birnessite-type MnO<sub>2</sub> on room-temperature oxidation of formaldehyde in air. *Appl. Catal., B* **2017**, *204*, 147-155.
- (75) Wang, J.; Zhang, G.; Zhang, P. Layered birnessite-type MnO<sub>2</sub> with surface pits for enhanced catalytic formaldehyde oxidation activity. *J. Mater. Chem. A* **2017**, *5* (12), 5719.
- (76) Bai, B.; Qiao, Q.; Li, J.; Hao, J. Synthesis of three dimensional ordered mesoporous MnO<sub>2</sub> and its catalytic performance in formaldehyde oxidation. *Chin. J. Catal.* **2016**, *37*, 27-31.
- (77) Zhou, L.; Zhang, J.; He, J.; Hu, Y.; Tian, H. Control over the morphology and structure of manganese oxide by tuning reaction conditions and catalytic performance for formaldehyde oxidation. *Mater. Res. Bull.* **2011**, *46* (10), 1714-1722.
- (78) Wu, Y.; Ma, M.; Zhang, B.; Gao, Y.; Lu, W.; Guo, Y. Controlled synthesis of porous Co<sub>3</sub>O<sub>4</sub> nanofibers by spiral electrospinning and their application for formaldehyde oxidation. *RSC Adv.* **2016**, *6*, 102127-102133.
- (79) Zeng, L.; Li, K.; Huang, F.; Zhu, X.; Li, H. Effects of Co<sub>3</sub>O<sub>4</sub> nanocatalyst morphology on CO oxidation: Synthesis process map and catalytic activity. *Chin. J. Catal.* **2016**, *37*, 908-922.
- (80) Huang, Y.; Long, B.; Tang, M.; Rui, Z.; Balogun, M.S.; Tong, Y.; Ji, H. Bifunctional catalytic material: An ultrastable and high-performance surface defect CeO<sub>2</sub> nanosheets for formaldehyde thermal oxidation and photocatalytic oxidation. *Appl. Catal., B* **2016**, *181*, 779-787.
- (81) Zeng, L.; Song, W.; Li, M.; Zeng, D.; Xie, C. Catalytic oxidation of formaldehyde on surface of H TiO<sub>2</sub>/H C TiO<sub>2</sub> without light illumination at room temperature. *Appl. Catal., B* **2014**, *147*, 490-498.
- (82) Zhou, L.; He, J.; Zhang, J.; He, Z.; Hu, Y.; Zhang, C.; He, H. Facile In-Situ Synthesis of Manganese Dioxide Nanosheets on Cellulose Fibers and their Application in Oxidative Decomposition of Formaldehyde. *J. Phys. Chem. C* **2011**, *15* (34), 16873-16878.
- (83) Imamura, S.; Shono, M.; Okamoto, N.; Hamada, A.; Ishida, S. Effect of cerium on the mobility of oxygen on manganese oxides. *Appl. Catal., A* **1996**, *142* (2), 279-288.
- (84) Luo, M. F.; Ma, J. M.; Lu, J. Q.; Song, Y. P.; Wang, Y.J. High-surface area CuO–CeO<sub>2</sub> catalysts prepared by a surfactant-templated method for low-temperature CO oxidation. *J. Catal.* **2007**, *246* (1), 52-59.
- (85) Ding, Z.Y.; Li, L.; Wade, D.; Gloyna, E.F. Supercritical water oxidation of NH<sub>3</sub> over a MnO<sub>2</sub>/CeO<sub>2</sub> catalyst *Ind. Eng. Chem. Res.* **1998**, *37* (5), 1707-1716.
- (86) Tang, X.; Li, Y.; Huang, X.; Xu, Y.; Zhu, H.; Wang, J.; Shen, W. MnO<sub>x</sub>–CeO<sub>2</sub> mixed oxide catalysts for complete oxidation of formaldehyde: effect of preparation method and calcination temperature. *Appl. Catal., B* **2006**, *62* (3), 265-273.
- (87) Lu, L.; Tian, H.; He, J.; Yang, Q. Graphene–MnO<sub>2</sub> Hybrid Nanostructure as a New Catalyst for Formaldehyde Oxidation. *J. Phys. Chem. C* **2016**, *120* (41), 23660-23668.

- (88) Lou, Y.; Cao, X.-M.; Lan, J.; Wang, L.; Dai, Q.; Guo, Y.; Ma, J.; Zhao, Z.; Guo, Y.; Hu, P.; Lu, G. Ultralow-temperature CO oxidation on an  $\text{In}_2\text{O}_3\text{--Co}_3\text{O}_4$  catalyst: a strategy to tune CO adsorption strength and oxygen activation simultaneously. *Chem. Commun. (Cambridge, U.K.)* **2014**, 50 (52), 6835-6838.
- (89) Wang, Z.; Pei, J.; Zhang, J. Catalytic oxidization of indoor formaldehyde at room temperature—Effect of operation conditions. *Build. Environ.* **2013**, 65, 49-57.
- (90) Wen, Y.; Tang, X.; Li, J.; Hao, J.; Wei, L.; Tang, X. Impact of synthesis method on catalytic performance of  $\text{MnO}_x\text{--SnO}_2$  for controlling formaldehyde emission. *Catal. Commun.* **2009**, 10 (8), 1157-1160.
- (91) Bai, L.; Wyrwalski, F.; Lamonier, J.F.; Khodakov, A.Y.; Monflier, E.; Ponchel, A. Effects of  $\beta$ -cyclodextrin introduction to zirconia supported-cobalt oxide catalysts: From molecule-ion associations to complete oxidation of formaldehyde. *Appl. Catal., B* **2013**, 138, 381-390.
- (92) Xuesong, L.; Jiqing, L.; Kun, Q.; Huang, W.; Mengfei, L. A comparative study of formaldehyde and carbon monoxide complete oxidation on  $\text{MnO}_x\text{--CeO}_2$  catalysts. *J. Rare Earths* **2009**, 27 (3), 418-424.
- (93) Li, J.W.; Pan, K.L.; Yu, S.J.; Yan, S.Y.; Chang, M.B. Removal of formaldehyde over  $\text{Mn}_x\text{Ce}_{1-x}\text{O}_2$  catalysts: Thermal catalytic oxidation versus ozone catalytic oxidation *J. Environ. Sci.* **2014**, 26, 2546-2553.
- (94) Zhu, L.; Wang, J.; Rong, S.; Wang, H.; Zhang, P. Cerium modified birnessite-type  $\text{MnO}_2$  for gaseous formaldehyde oxidation at low temperature. *Appl. Catal., B* **2017**, 211, 212-221.
- (95) Shi, C.; Wang, Y.; Zhu, A.; Chen, B.; Au, C.  $\text{Mn}_x\text{Co}_{3-x}\text{O}_4$  solid solution as high-efficient catalysts for low-temperature oxidation of formaldehyde. *Catal. Commun.* **2012**, 28, 18-22.
- (96) Lu, S.; Li, K.; Huang, F.; Chen, C.; Sun, B. Efficient  $\text{MnO}_x\text{--Co}_3\text{O}_4\text{--CeO}_2$  catalysts for formaldehyde elimination. *Appl. Surf. Sci.* **2017**, 400, 277-282.
- (97) Sidheswaran, M. A.; Destailhats, H.; Sullivan, D. P.; Larsen, J.; Fisk, W. J. Quantitative room-temperature mineralization of airborne formaldehyde using manganese oxide catalysts. *Appl. Catal., B* **2011**, 107 (1), 34-41.
- (98) Li, J., Zhang, P., Wang, J. and Wang, M. Birnessite-Type Manganese Oxide on Granular Activated Carbon for Formaldehyde Removal at Room Temperature. *J. Phys. Chem. C* **2016**, 120 (42), 24121-24129.
- (99) Bai, B.; Li, J.; Hao, J. 1D- $\text{MnO}_2$ , 2D- $\text{MnO}_2$  and 3D- $\text{MnO}_2$  for low-temperature oxidation of ethanol. *Appl. Catal., B* **2015**, 164, 241-250.
- (100) Sun, Y.; Zhang, W.; Li, D.; Gao, L.; Hou, C.; Zhang, Y.; Liu, Y. Facile synthesis of  $\text{MnO}_2/\text{rGO}/\text{Ni}$  composite foam with excellent pseudocapacitive behavior for supercapacitors. *J. Alloys Compd.* **2015**, 649, 579-584.
- (101) Zhang, C.; He, H.; Tanaka, K.I. Catalytic performance and mechanism of a  $\text{Pt}/\text{TiO}_2$  catalyst for the oxidation of formaldehyde at room temperature. *Appl. Catal., B* **2006**, 65 (1), 37-43.

- 1275 (102) Chen, B.B.; Zhu, X. B.; Crocker, M.; Wang, Y.; Shi, C. FeO x-supported gold catalysts for  
1276 catalytic removal of formaldehyde at room temperature. *Appl. Catal., B* **2014**, *154*, 73-81.  
1277  
1278 (103) Yu, J.; Li, X.; Xu, Z.; Xiao, W. NaOH-Modified Ceramic Honeycomb with Enhanced  
1279 Formaldehyde Adsorption and Removal Performance. *Environ. Sci. Technol.* **2013**, *47* (17),  
1280 9928-9933.